CHEMISTRY & SUSTAINABILITY

CHEMSUSCHEM

ENERGY & MATERIALS

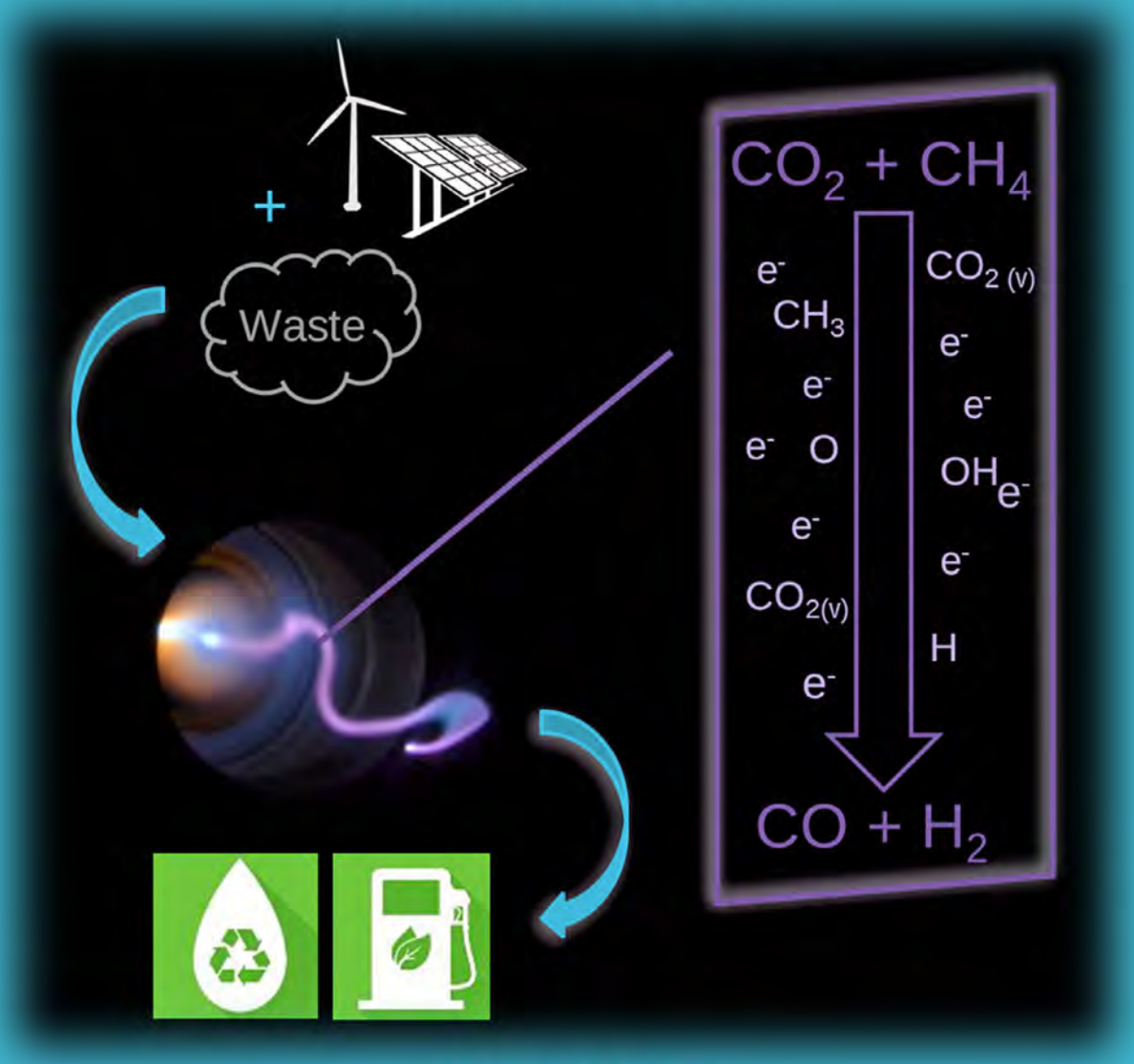

20/2017

Cover Feature:

Cleiren et al.

Dry Reforming of Methane in a Gliding Arc Plasmatron: Towards a Better Understanding of the Plasma Chemistry

A Journal of ChemPubSoc Europe

WILEY-VCH

www.chemsuschem.org

COVER PICTURE

*E. Cleiren, S. Heijkers, M. Ramakers,**
*A. Bogaerts**

■■ – ■■

Dry Reforming of Methane in a Gliding Arc Plasmatron: Towards a Better Understanding of the Plasma Chemistry

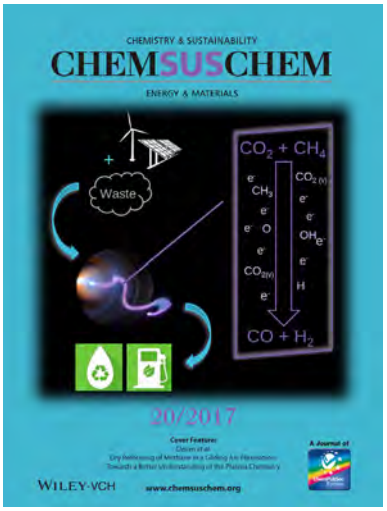

The Cover Feature shows a gliding arc plasmatron (a new type of plasma reactor) that can convert methane through dry reforming into useful fuels and compounds. This process can fit into the "cradle-to-cradle" concept, as waste (CO_2 and CH_4) can be converted into raw materials (syngas) for the chemical industry using renewable energy. A non-thermal plasma can accomplish this reaction in an energy efficient way because only the electrons are heated and they activate the gas molecules. A gliding-arc plasma is very promising as it operates at atmospheric pressure and yields a good energy efficiency. More information can be found in the Full Paper by Cleiren et al.

ChemPubSoc Europe
DOI: 10.1002/cssc.201701274
CHEMSUSCHEM Full Papers

Dry Reforming of Methane in a Gliding Arc Plasmatron: Towards a Better Understanding of the Plasma Chemistry

Emelie Cleiren, Stijn Heijkers, Marleen Ramakers,* and Annemie Bogaerts*[a]

Dry reforming of methane (DRM) in a gliding arc plasmatron is studied for different CH_4 fractions in the mixture. The CO_2 and CH_4 conversions reach their highest values of approximately 18 and 10%, respectively, at 25% CH_4 in the gas mixture, corresponding to an overall energy cost of 10 kJ L^{-1} (or 2.5 eV per molecule) and an energy efficiency of 66%. CO and H_2 are the major products, with the formation of smaller fractions of C_2H_x ($x=2$, 4, or 6) compounds and H_2O. A chemical kinetics model is used to investigate the underlying chemical processes. The calculated CO_2 and CH_4 conversion and the energy efficiency are in good agreement with the experimental data. The model calculations reveal that the reaction of CO_2 (mainly at vibrationally excited levels) with H radicals is mainly responsible for the CO_2 conversion, especially at higher CH_4 fractions in the mixture, which explains why the CO_2 conversion increases with increasing CH_4 fraction. The main process responsible for CH_4 conversion is the reaction with OH radicals. The excellent energy efficiency can be explained by the non-equilibrium character of the plasma, in which the electrons mainly activate the gas molecules, and by the important role of the vibrational kinetics of CO_2. The results demonstrate that a gliding arc plasmatron is very promising for DRM.

Introduction

One possible strategy to reduce greenhouse gas emissions is to convert CO_2 and other greenhouse gases such as CH_4 into value-added chemicals. In the so-called dry reforming of methane (DRM), CO_2 and CH_4 react together to form syngas (CO/H_2 mixture), resulting in the conversion of two greenhouse gases simultaneously. However, classical catalytic DRM faces problems such as the need for high temperatures and catalyst poisoning by carbon deposition. Therefore, in recent years, several novel technologies have been proposed; one of these is plasma technology.[1,2]

Plasma is (partially) ionized gas, sometimes seen as the fourth state of matter. A gas discharge plasma is typically created by applying an electric field to a gas, which results in a cocktail of reactive species including molecules, radicals, atoms, ions, electrons, and excited species that can all interact with each other, providing the basis for a variety of applications.[3] Plasma technology is of particular interest for energy-efficient gas conversion, because the gas must not be heated as a whole for the reactions to take place. Indeed, the electrons are selectively heated by the electric field owing to their small mass. These electrons subsequently activate the gas molecules by electron impact excitation, ionization, and dissociation, creating reactive species that can easily form new molecules.

In recent years, many different types of plasmas have been investigated for CO_2 conversion, including DRM. A very recent comprehensive overview of the capabilities and limitations of the various plasma types is provided in Ref. [2]. A gliding arc (GA) plasma is very promising because it operates at atmospheric pressure and yields a good energy efficiency owing to the active contribution of the CO_2 vibrational levels in the dissociation process.[4] A classical GA is created by applying a potential difference between two flat diverging electrodes. The arc is created at the shortest interelectrode gap and is dragged by the gas flow towards larger interelectrode gaps until it extinguishes and a new arc is again formed at the shortest gap, repeating the cycle. However, classical GA faces limitations such as limited gas conversion because of the short residence time of the gas inside the plasma column.[5–7] Therefore, in recent years, some new designs have been developed based on cylindrical electrodes and a tangential gas inlet, which yields a vortex flow and allows the gas to stay inside the plasma for a longer time, resulting in a higher conversion. One such type of novel GA is the so-called gliding arc plasmatron (GAP), developed at Drexel University by Nunnally et al.[8] The GAP has been demonstrated to yield good energy efficiency for pure CO_2 conversion[8,9] but has not been applied for DRM. However, other cylindrical (e.g., so-called tornado-type or rotating) GA designs have been applied for DRM and have exhibited very promising results.[10–15]

In this study, we investigated for the first time the performance of the GAP for DRM. Our experiments are supported by chemical kinetics modeling to understand the underlying chemical processes. Chemical kinetics modeling is very useful for this purpose and has been applied to DRM in another type

[a] E. Cleiren, S. Heijkers, M. Ramakers, Prof. Dr. A. Bogaerts
Department of Chemistry, Research Group PLASMANT
University of Antwerp, Universiteitsplein 1, 2610 Wilrijk (Belgium)
E-mail: marleen.ramakers@uantwerpen.be
annemie.bogaerts@uantwerpen.be

Supporting information and the ORCID identification number(s) for the author(s) of this article can be found under https://doi.org/10.1002/cssc.201701274.

of plasma, i.e., the plasma generated by a dielectric barrier discharge (DBD),[16,17] but not in plasma generated by a GA.

Results and Discussion

Measured conversion, energy efficiency, and energy cost

We investigated the CO_2 and CH_4 conversion, energy efficiency, and energy cost, as well as the product selectivities (see next section) as a function of the CH_4 fraction in the gas mixture (from 0 to 25%) for a gas flow rate of 10 L min^{-1}. We were limited to a maximum CH_4 fraction of 25% in the current setup because the plasma became unstable for larger fractions owing to limitations of the power supply. The plasma power was approximately 500 W in the entire range of CH_4 fractions, yielding a specific energy input (SEI) of approximately 3 kJ L^{-1} (or 0.75 eV per molecule; Figure S1 in the Supporting Information).

Figure 1a and b illustrate the measured CO_2 and CH_4 conversion as a function of CH_4 fraction in the mixture. The absolute CO_2 conversion increased from 7.5 to 24% upon increasing CH_4 fraction, whereas the absolute CH_4 conversion dropped from 61 to 42% (Figure 1a). The CH_4 conversion was much higher than the CO_2 conversion, which was attributed to the

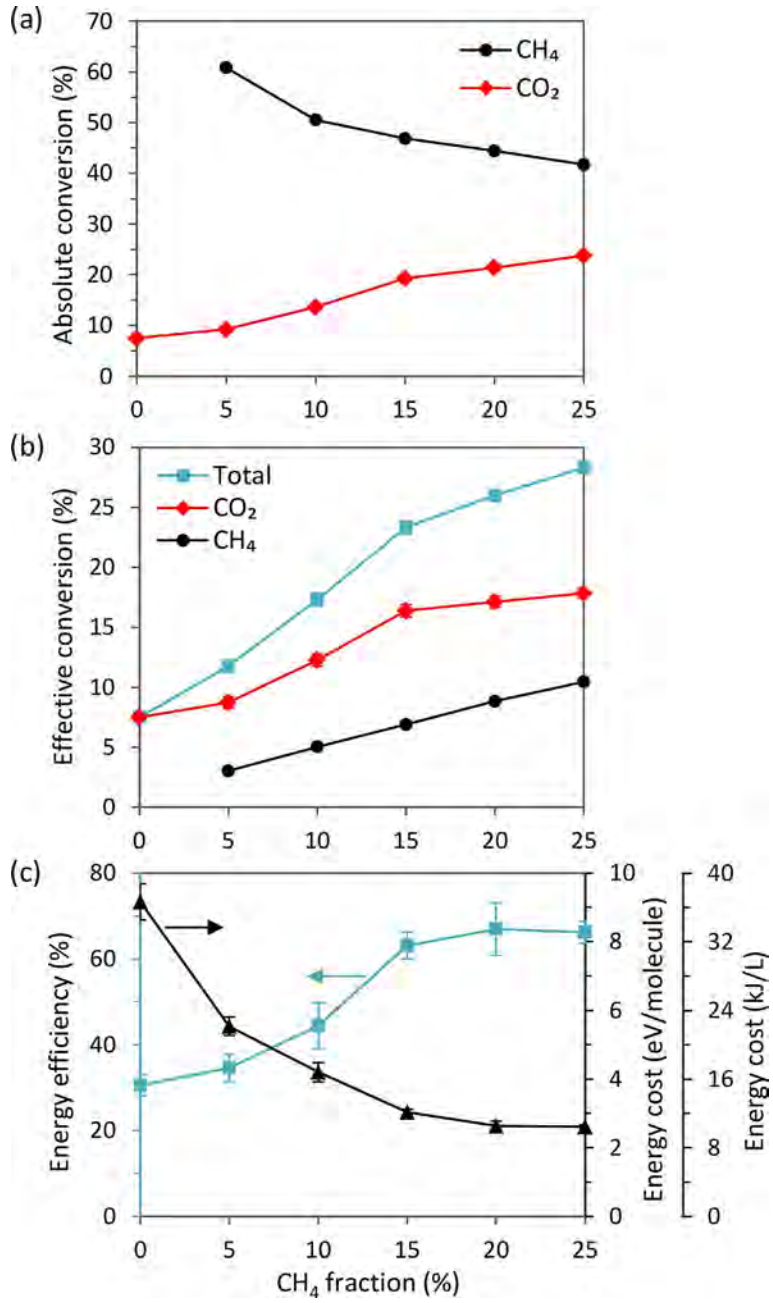

Figure 1. Absolute (a) and effective (b) conversion of CO_2 and CH_4, as well as the total conversion (b), and overall energy efficiency and energy cost (c), as a function of CH_4 fraction in the mixture. The error bars are included in the graphs, but are too small to be visible in (a) and (b).

lower bond dissociation energy of C–H (4.48 eV) compared to C=O (5.52 eV), making te dissociation of CH_4 easier than for CO_2.

The effective conversion of CO_2 and CH_4 in the mixture was obtained by multiplying the absolute conversion with the fraction of the component in the mixture (Figure 1b). The effective CO_2 and CH_4 conversion both increase with increasing CH_4 fraction. Indeed, the rising CH_4 fraction compensated for the lower absolute CH_4 conversion, whereas the lower CO_2 fraction in the mixture was not important enough to compensate for the higher absolute CO_2 conversion upon the addition of CH_4 to the mixture. The underlying mechanisms explaining these trends are discussed below. Consequently, the overall conversion also increased from 7.5 to approximately 30% upon the addition of CH_4 to the mixture. These trends agreed well with results obtained in a tornado-type GA plasma.[10]

The energy efficiency and energy cost upon increasing CH_4 fraction are plotted in Figure 1c. The energy efficiency follows the rising trend of the overall conversion, whereas the energy cost follows the opposite trend. This is logical because the energy efficiency and energy cost are linearly and inversely proportional to the overall conversion, respectively, and they are further determined by the SEI (see Formulae 9 and 10 in the Supporting Information); the SEI is more or less constant in the entire range of CH_4 fractions (Figure S1). The rising trend in energy efficiency was most striking up to 15% CH_4 fraction, increasing from 30% in pure CO_2 to above 60% between 15 and 25% CH_4. The energy cost dropped from 37 to 10 kJ L^{-1} (or from 9.3 to 2.6 eV per molecule) upon increasing the CH_4 fraction. The trends of rising energy efficiency and decreasing energy cost were accompanied by a slight drop in the temperature of the gas flowing out of the GAP reactor, from 120 °C to 103 °C at 0% and 25% CH_4 fraction, respectively. Clearly, less energy was lost to gas heating and more energy could effectively be used for the conversion.

The combined values of the conversion, energy efficiency, and energy cost were much better than the typical values obtained in DBDs, which are the most commonly used plasmas for DRM. Indeed, DBDs typically yield maximum conversions of a few % up to 60% (with a few exceptions up to 80% for packed-bed DBDs), but the corresponding energy cost is between 20 and 100 eV per molecule (with some lower and higher exceptions for packed bed DBDs).[17–44] We compared the literature values for the energy cost instead of the energy efficiency because for the latter we need to account for all formed products (and their enthalpy of formation; cf. Formula 9 in the Supporting Information); in the literature, typically, only the selectivity towards the syngas components (and sometimes light hydrocarbons) is reported, making a comparison based on energy efficiencies not very reliable. However, comparison based on the energy cost can provide the same insights in the performance of our GAP compared to other results in the literature.

Microwave (MW) plasmas are quite promising for pure CO_2 splitting, with energy efficiencies of up to 50% at a conversion of up to 26%;[45,46] however, these values are typically reached at reduced pressure, which is less convenient for industrial applications, and the energy cost of vacuum systems would have to be added to the overall energy cost. Moreover, the number of studies on DRM in a MW plasma is very limited. A pulsed MW plasma was able to demonstrate an absolute CH_4 and CO_2 conversion of 71% and 69%, respectively, with an energy cost of 6.5 eV per molecule.[47] Comparing these results with our GAP, for which we obtained an absolute CH_4 and CO_2 conversion of up to 61% and 24%, respectively (cf. Figure 1a above), the conversion was higher in this MW plasma but the energy cost was also double the best value reached in our experiments. Another study of continuous MW plasma yielded similar maximum conversions as in the pulsed MW plasma, but with a higher power (1.5 kW), and thus a very high energy cost of up to 343 eV per molecule.[48]

For GA plasmas, maximum conversions in the range of 30–50% have been reported, with energy costs as low as 1–2 eV per molecule.[10–15,49–54] The best reported result was obtained for a rotating GA reactor, which yielded a total conversion of 39% with an energy cost of 1 eV per molecule,[11] which is somewhat better than our results.

Other types of plasmas have also been investigated for DRM. In corona discharges, maximum conversions between 10 and 90% have been reached, with energy costs between 4 and 100 eV per molecule.[55–62] The best combined result was a conversion of 44% with an energy cost of 5.2 eV per molecule.[56] In spark discharges, the minimum energy cost has been reported to be approximately 3–10 eV per molecule for conversions between 10 and 85%,[63–70] with the best total conversion of 85% with an energy cost of 3.2 eV per molecule.[63] Atmospheric pressure glow discharges also seem to be promising for DRM, with maximum conversions of 35–85% and energy costs of 1–60 eV per molecule.[71–73] The best result is a total conversion of 89% with an energy cost of only 1.2 eV per molecule.[72] Finally, nanosecond-pulsed plasmas provided conversions between 1 and 60% for energy costs between 3 and 100 eV per molecule.[74–79]

Clearly, the GAP is among the most promising types of plasmas for DRM in terms of energy cost or energy efficiency. In Ref. [2], a maximum energy cost of 4.27 eV per molecule corresponding to a minimum energy efficiency of 60% (assuming that syngas was the only product formed) was proposed as the target for plasma-based DRM to become industrially competitive with classical and other novel conversion technologies. Figure 1c illustrates that we reached this target with our GAP if the CH_4 fraction in the gas mixture was sufficiently high. This good result was attributed to the important role of the vibrational levels of CO_2 for energy-efficient conversion, as explained below.

Measured product selectivities

The major DRM products detected in our GAP were CO and H_2, alongside, to a much lower extent, O_2, H_2O, and C_2H_x ($x = 2$, 4, or 6) hydrocarbons. Our modeling calculations reveal that other products can also be formed in this gas mixture, as discussed below. Figure 2a illustrates the (H- and O-based) selectivities of H_2 and O_2 as a function of the CH_4 fraction. The re-

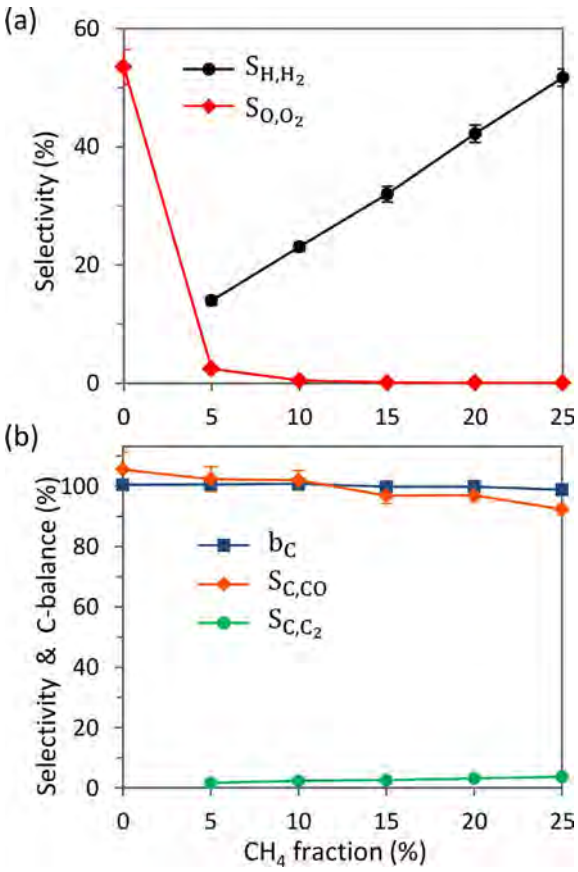

Figure 2. H- and O-based selectivities (a) and C-based selectivities (in which C_2 is the sum of C_2H_6, C_2H_4, and C_2H_2) as well as the C balance (b) as a function of CH_4 fraction in the mixture.

maining H and O atoms give rise to higher hydrocarbons (C_2H_x) and H_2O, and to CO and H_2O, respectively, and maybe to some minor oxygenated compounds that could not be detected. The strong drop in O-based selectivity of O_2 (S_{O,O_2}) upon addition of 5% CH_4 indicated that the O atoms, which were mainly converted into O_2 (and CO) in pure CO_2 splitting, were converted into other compounds upon addition of a H-source, so that almost no O_2 was formed anymore. This is discussed in more detail below. Furthermore, it is clear from Figure 2a that the selectivity towards H_2 increased, which was desirable as H_2 is a component of syngas. At a low CH_4/CO_2 ratio, the H-based selectivity towards H_2O will be higher.[2]

Figure 2b presents the C-based selectivities as well as the C-balance, which was 100%. The fact that the C-based selectivity of CO ($S_{C,CO}$) was sometimes higher than the C-balance was probably due to the error associated with this selectivity. CO was clearly the dominant product. The slight drop in $S_{C,CO}$ upon increasing CH_4 fraction was due to a rise in the formation of other C-based products such as C_2 components. However, the rise in S_{C,C_2} from 2 to 4% (Figure 2b) was not sufficient to compensate for the drop of 13% (with an uncertainty of 6%) in $S_{C,CO}$, which indicated that other C-based compounds that were not detected by GC were formed.

The two main components formed were H_2 and CO (syngas). The H_2/CO ratio increased slightly more than linearly upon increasing CH_4 fraction, from 0.08 at 5% CH_4 to 0.44 at 25% CH_4 (Figure S2). This was logical because CH_4 was the only source of H in the mixture. The H_2/CO ratio was strongly affected by the gas mixing ratio and could be easily tuned by this parameter to reach optimum values for subsequent Fischer–Tropsch (FT) or methanol synthesis. However, the current CO and H_2 yields might still be too low for FT or methanol synthesis, which require high yields of CO and H_2 feed gas, as obtained from DRM. This is because the conversion in our current setup is still rather low. In the future, we aim to optimize our setup to improve the conversion.

Comparison of measured and calculated conversion and energy efficiency

We developed a chemical kinetics model to investigate the underlying mechanisms of DRM in our GAP, as explained below and in the Supporting Information. Before we used this model for a deeper analysis, we validated it against the experimental data for conversion and energy efficiency. Figure 3 illustrates the CO_2 (Figure 3a) and CH_4 (Figure 3b) conversion as a function of the CH_4 fraction in the mixture for an input power of 500 W (SEI = 0.75 eV per molecule) and gas flow rate of 10 L min^{-1}. As explained below, the arc was stabilized in the center of the GAP reactor, and only a fraction of the gas (i.e., 14.8%; for details, see below and the Supporting Information) passed through this arc column. However, we did not only consider the conversion inside the arc column but also in a certain region around the actual arc column that is still at a rather high temperature, thus allowing some thermal conversion to take place. Both contributions are indicated in Figure 3a and b with dashed lines. Adding both contributions yields the total conversion, which was compared with the measured conversion. Both the rising trend in CO_2 conversion (Figure 3a) and the drop in CH_4 conversion (Figure 3b) were correctly predicted by the model and the absolute values were in very good agreement.

As evident from Figure 3a and b, only accounting for the conversion in the arc column would underestimate the total conversion, especially for CH_4, for which the thermal conversion outside the arc column appeared to be even higher than the plasma conversion. This was attributed to the lower C–H bond dissociation energy, which allowed thermal conversion to occur at lower temperatures. The relative contributions of the conversion inside the arc and the thermal conversion in the area around the arc are plotted for both CO_2 and CH_4 in Figure S3.

Furthermore, Figure 3b indicates that the CH_4 conversion inside the arc was constant at 14.8%, independent from the CH_4 fraction in the mixture. The reason was that the CH_4 conversion inside the arc was in fact 100%, but the overall contribution of the arc was limited by the fraction of gas that passed through the arc, which was predicted to be 14.8% (see a more detailed discussion below).

Figure 3c illustrates the measured and calculated values of the energy efficiency as a function of the CH_4 fraction. Again, the agreement was very good, with relative differences be-

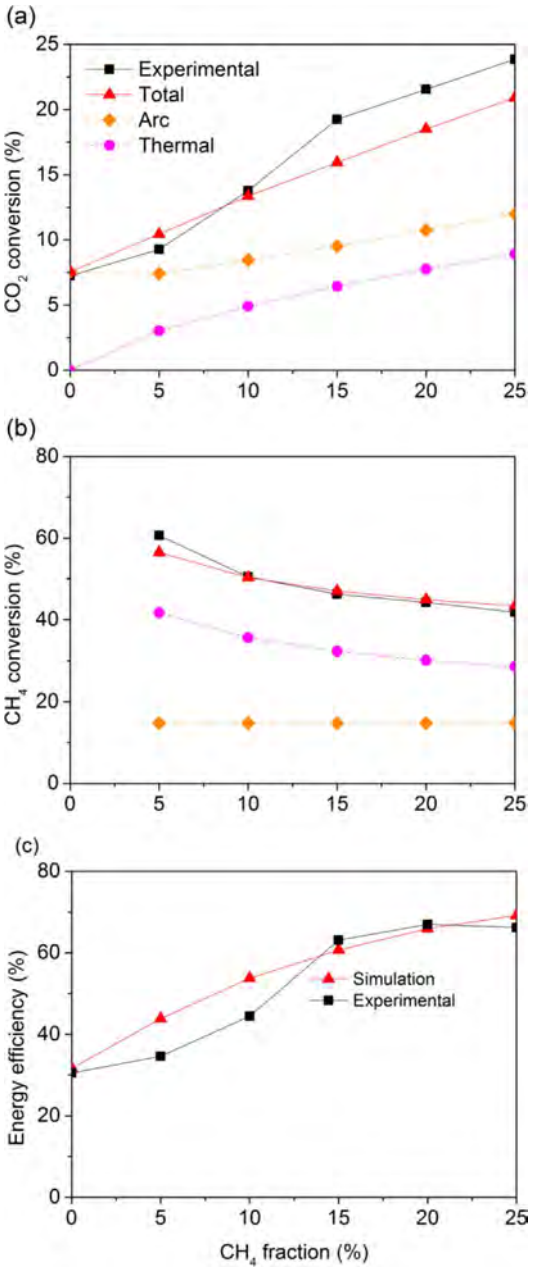

Figure 3. Measured and calculated CO_2 conversion (a) and CH_4 conversion (b), as well as energy efficiency (c) as a function of the CH_4 fraction in the mixture. The individual contributions of the conversion inside the arc and in the thermal area around the arc are indicated as dashed lines in (a) and (b).

tween 1.5 and 27% and an average difference of 10% between the values. The rising trend was not exactly the same at low CH_4 fraction, which may indicate that the thermal conversion was somewhat overestimated at 5 and 10% CH_4 in the mixture. Indeed, the model simply assumes the same area around the arc column at which thermal conversion can take place, but this area will most probably be smaller at low CH_4 fractions because CH_4 gives rise to a somewhat higher temperature. Of course, the assumptions made about the thermal conversion in a fixed area around the arc are somewhat rough, owing to the inherent nature of the 0D chemical kinetics model. A more accurate description would require full 3D calculations;[80,81] however, this would result in excessively long calculation times when incorporating the complex CO_2/CH_4 chemistry. Nevertheless, despite the approximations that need to be made in the 0D model, the agreement was quite satisfactory. In general, the model provides quite realistic predictions of the CO_2 and CH_4 conversion and the energy efficiency, which could be used to investigate the underlying mechanisms.

Calculated plasma characteristics

Before analyzing the underlying chemical reactions of the CO_2 and CH_4 conversion, we first provide information about the plasma characteristics in the arc column, which helps with the understanding of the mechanisms. The important characteristics inside the arc column, defining the plasma chemistry and thus the CO_2 and CH_4 conversion, are the gas temperature, electron temperature, density, and the vibrational temperature, which gives information on the degree of vibrational excitation.

In principle, the gas temperature can be calculated in the model (Supporting Information), but in this study we assume certain values based on 3D fluid dynamics simulations[80,81] and reported data.[82] Indeed, to obtain realistic calculations with this 0D model, we would need more accurate data on the energy released by some chemical reactions and on the effect of vibration–translation relaxation of the CO_2 vibrational levels upon collision with CH_4; these data were not available in the literature. Furthermore, the effect of turbulent heat conductivity has also been demonstrated to be very critical in a GAP, yielding a significant drop in gas temperature;[81] this effect cannot be accounted for in a 0D model.

In Figure 4a, the assumed gas temperature profile inside the arc column (solid line) and in the thermal area around the arc (dashed line) are plotted as a function of position in the reactor. These values were assumed to be independent of the gas mixing ratio, which might be an approximation but subtle differences for different gas mixtures would lie within the uncertainty of these values. The gas entered the arc column at room temperature but was quickly heated to approximately 3500 K after 0.5 cm. The temperature of the gas in the thermal area around the arc column increased slower, up to a value of 2700 K after approximately 1.2 cm. At this temperature, thermal conversion of CO_2 and CH_4 does indeed take place, as revealed by thermal conversion calculations.[2]

The calculated electron temperature and density are plotted in Figure 4b and c for different CH_4 fractions in the mixture. At the beginning of the arc column the electron density was still low, so that all the applied electrical energy was distributed over a limited number of electrons, which explains the high electron temperature at the beginning of the arc column. This electron temperature was slightly higher than expected for a GA,[1] but it did not really affect the calculated plasma chemistry because of the low electron density in this region. After approximately 0.5 cm, the electron density increased, and as a consequence, the electron temperature dropped to values of

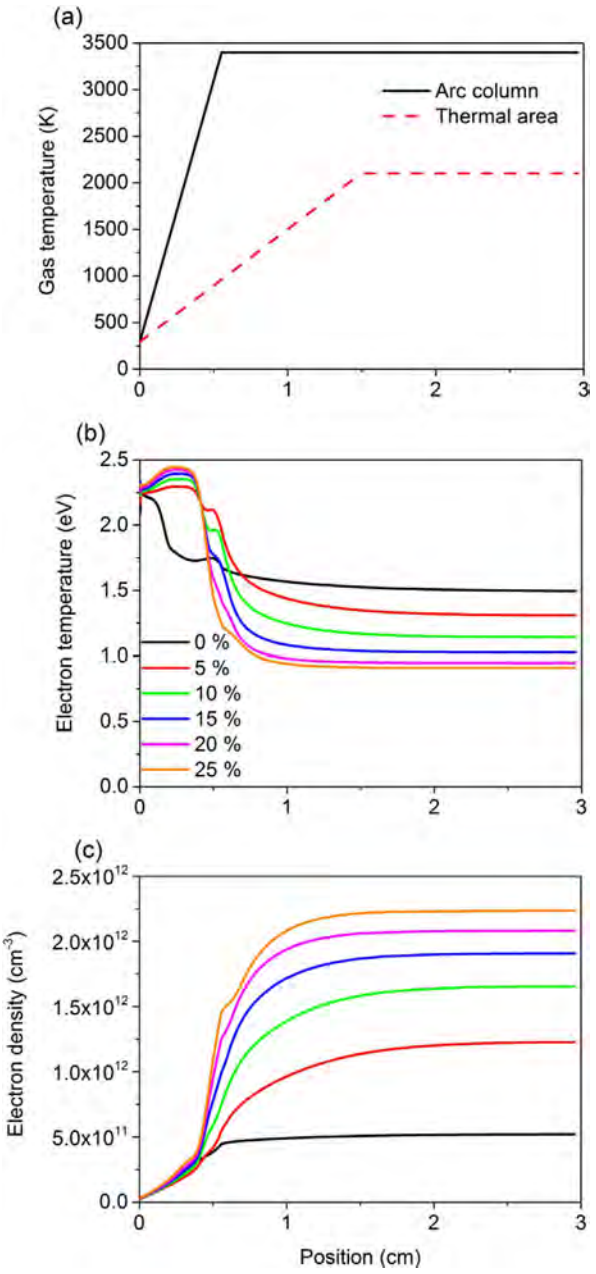

Figure 4. Assumed gas temperature inside the arc column (solid line) and in the thermal area around the arc (dashed line) (a), as well as calculated electron temperature (b) and electron density (c) for different CH_4 fractions in the mixture as a function of position in the arc. The gas temperature is assumed to be independent from the gas composition.

approximately 1.0–1.5 eV (for different CH_4 fractions), which were typical values expected for a GA.[1] The electron temperature slightly dropped if the CH_4 fraction in the mixture was higher, which was due to the slightly lower values of the reduced electric field (i.e., ratio of electric field over gas density, E/n, typically expressed in Td; 1 Td = 10^{-21} V m^2). In the model, the latter was calculated to be 57 Td and 22 Td for the 0% and 25% CH_4 fractions, respectively. Furthermore, a higher CH_4 concentration yielded a higher electron density owing to the lower ionization potential of CH_4 (12.61 eV) versus CO_2 (13.78 eV).

Besides the gas temperature and electron temperature, the vibrational temperature is an important characteristic of the GAP because the vibrational levels play a key role in energy-efficient CO_2 dissociation. To calculate the vibrational temperature, we plotted the vibrational distribution function (VDF) of the 21 asymmetric mode levels of CO_2 (v_1–v_{21}), as well as the 4 effective symmetric mode levels (v_a–v_d; for details about these levels and their notation, see the Supporting Information), both inside the arc column and in the thermal area around the arc (Figure 5). According to our calculations, the VDF was independent from the CH_4 fraction in the mixture. A faster drop of the VDF for the asymmetric mode levels in the thermal region yielded a somewhat lower vibrational temperature (T_v). The latter is a measure of the degree of vibrational excitation and can be calculated as follows from the VDF, in case of a Boltzmann distribution for the asymmetric mode levels [Eq. (1)]:

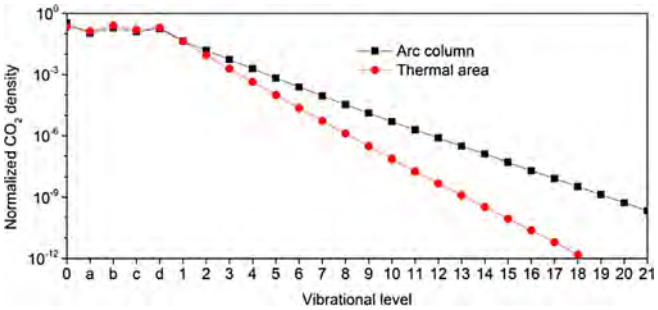

Figure 5. Vibrational distribution functions (VDFs) of all vibrational levels of CO_2 included in the model, both in the arc column and in the thermal area around the arc. These VDFs were found to be the same for all gas mix ratios investigated. The notations of the vibrational levels are explained in the Supporting Information.

$$T_v = \frac{1}{21}\sum_{n=1}^{21}\frac{-E_n}{\ln\left(\frac{n_n}{n_0}\right)} \quad (1)$$

in which E_n is the energy of the nth asymmetric vibrational level of CO_2, n_n is the density of this level, and n_0 is the density of CO_2 in the ground state.

The vibrational temperature of the asymmetric mode levels was calculated to be approximately 3400 K inside the arc and approximately 2800 K in the thermal area around the arc, which (more or less) corresponds to the gas temperature adopted in both regions. This indicated that the VDF was quasi-thermal. Indeed, no overpopulation of the higher vibrational levels was observed in Figure 5. The same behavior was also observed in a GAP and a classical GA operating in pure CO_2,[5,83–85] as well as in MW plasma in pure CO_2 operating at atmospheric pressure.[86] Overpopulation of the higher levels has only been observed in a MW plasma at reduced pressure[86–89] because of the less important role of thermalization owing to vibration–translation relaxation.

The electron temperature is much higher than the gas temperature and the vibrational temperature (i.e., 1–1.55 eV, or

11 000–18 000 K vs. 3400–3500 K in the arc). This indicated the non-equilibrium character of the GAP and explains why the CO_2 and CH_4 conversions in the GAP were quite energy efficient, because the electrons were energetic enough to activate the gas by ionization, excitation, and dissociation. Nevertheless, if the vibrational temperature was higher than the gas temperature owing to overpopulation of the higher vibrational levels of CO_2, the CO_2 conversion would still be more energy efficient. A possible way to realize such overpopulation of the higher vibrational levels could be by operating at a lower gas temperature in combination with a higher power,[86] or operating at reduced pressure, as demonstrated for MW plasmas.[86–89] However, the latter is not beneficial for industrial applications and the cost of the vacuum system would also have to be accounted for in the overall energy efficiency.

Calculated species densities inside the plasma

The densities of the most important plasma species at the end of the arc column were plotted as a function of the CH_4 fraction in the mixture (Figure 6). We did not make a distinction between ground state and vibrationally or electronically excited levels of the various molecules and plotted the sum of both. 84% of the CO_2 molecules were found in the vibrationally excited levels. For CO, O_2, H_2, and CH_4, this fraction was much lower, i.e., 39%, 24%, 4%, and <1%, respectively, and

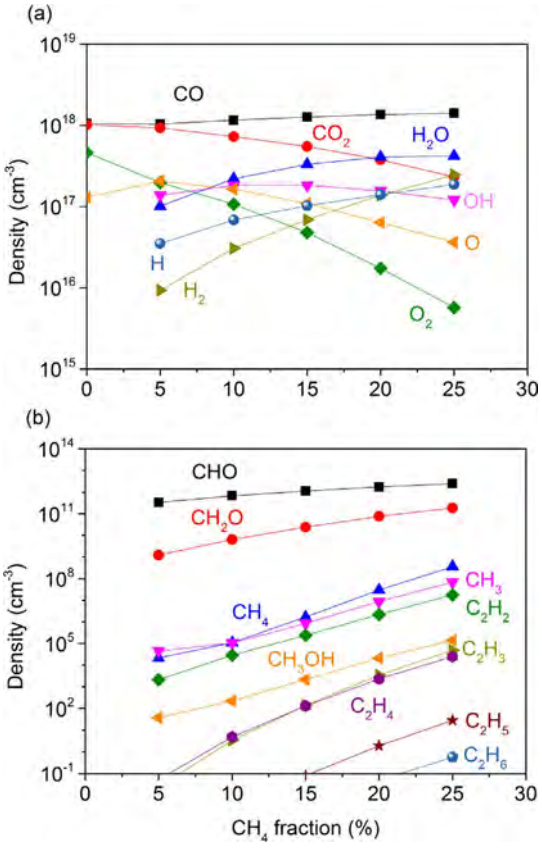

Figure 6. Densities of the most important plasma species at the end of the arc column as a function of the CH_4 fraction in the mixture.

the fraction of electronically excited levels was also of minor importance. For other molecules in the mixture, no vibrational levels were accounted for (for details, see Tables S1 and S2).

The CO density was higher than the CO_2 density (Figure 6a), which indicated that most of the CO_2 was converted inside the arc column. However, for the overall conversion, we also had to account for the fraction of CO_2 gas than could not pass through the arc column, which explains why the overall conversion was much lower (cf. Figure 3). The same applies to the CH_4 density (Figure 6b), which was extremely low, as it was entirely converted into H_2 and higher hydrocarbons inside the arc column. The densities of O_2 and O were only significant in pure CO_2 and dropped considerably if the CH_4 fraction in the mixture was higher. This drop was also reflected in the measured O-based selectivity of O_2 (cf. Figure 2). Indeed, the O atoms, which recombine into O_2 (and CO) in the pure CO_2 plasma, recombine with H atoms originating from CH_4 into OH, H_2O, CH_3OH, and CH_2O, although the densities of the two latter species were still quite low (cf. Figure 6b. The most important products were CO and H_2, along with H_2O. The predominant formation of CO and H_2 could also be deduced from our experimental selectivities (Figure 2). However, the H_2O could not be quantified owing to a very broad band in our GC chromatogram. Nevertheless, the sum of the O-based selectivities was not 100%, which indicated that a considerable fraction of H_2O was formed. In addition, oxygenated compounds could be formed but our model revealed that their densities were much lower. A catalyst is most probably needed to obtain higher concentrations of these compounds, which we will investigate in the future.

Upon increasing the CH_4 fraction in the mixture, more H atoms were converted into H_2, as is clear from Figure 6a. Furthermore, Figure 6b revealed the following trend for the C_2 compounds: $C_2H_6 < C_2H_5 < C_2H_4 < C_2H_3 < C_2H_2$. This was in contrast to the results observed for a DBD, in which C_2H_6 was obtained with the highest concentration of all hydrocarbons owing to recombination of CH_3 radicals.[25] This can probably be explained by the higher temperature in the GAP, which led to greater dehydrogenation of C_2H_6 upon electron impact reactions or collisions with O atoms.[49]

Chemical kinetics analysis of the underlying processes

The kinetic model allowed us to obtain a better insight in the loss and formation processes of CO_2 and CH_4, from which we could explain the experimental trends of the CO_2 and CH_4 conversions upon increasing CH_4 fraction in the mixture (cf. Figure 1). A detailed analysis of these loss and formation processes is presented in Figures S4–S7. Based on this analysis, we plotted the relative contributions of the main processes responsible for the (net) conversion of CO_2 and CH_4 as a function of the CH_4 fraction in the mixture (Figure 7a, b).

Figure 7a illustrates that without the addition of CH_4, the reaction of CO_2 (mainly in the vibrational levels; see the Supporting Information) with either O atoms or any other molecules (indicated as M) was most important for the conversion of CO_2. The reaction with O atoms was dominant at 5% CH_4 in the

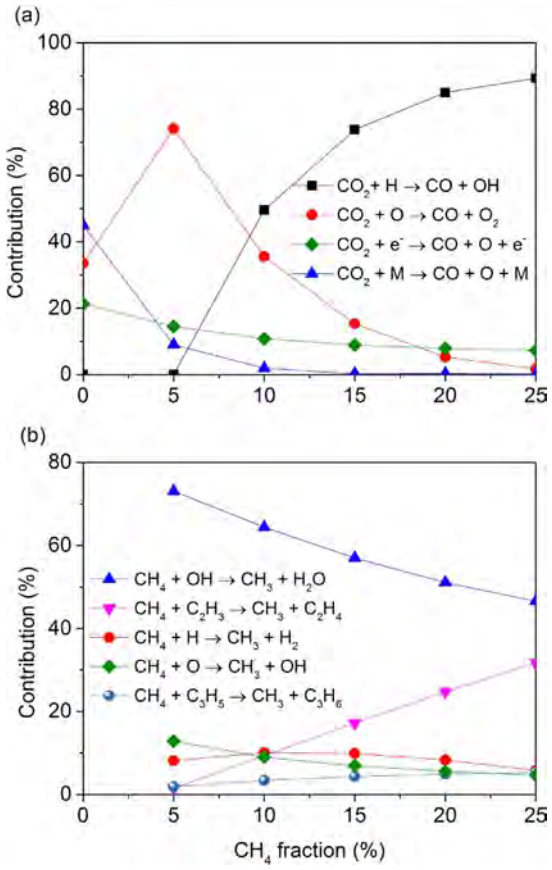

Figure 7. Relative contributions of the main processes responsible for the (net) conversion of CO_2 (a) and CH_4 (b) as a function of CH_4 fraction in the mixture.

mixture, but at larger CH_4 fractions both processes were less important, whereas the reaction of CO_2 (again mainly in the vibrational levels; see the Supporting Information) with H atoms was dominant, with contributions of more than 80%. Electron impact dissociation, both from the CO_2 ground state and vibrational levels (see the Supporting Information), contributed for approximately 10–20% of the total CO_2 conversion. The net CO_2 loss rate increased upon increasing CH_4 fraction (Figure S5), which was attributed to the increasing importance of the reaction with H atoms. Hence, the dissociation of CO_2 upon collision with H atoms explains why the CO_2 conversion increased upon increasing CH_4 fraction in the mixture (cf. Figure 1).

As shown in Figure S4, the backward reaction of the most important loss process for CO_2 in the CO_2/CH_4 mixture ($CO_2 + H \rightarrow CO + OH$), i.e., the reaction of CO with OH radicals to form CO_2 and H atoms, was nearly equally important as the loss (i.e., forward) reaction, especially at low CH_4 fractions. Therefore, this reaction did not contribute to CO_2 conversion at 5% CH_4 in the mixture and was only important at larger CH_4 fractions, as is clear from Figure 7. This reverse reaction was also the limiting factor in CO_2 conversion in a DBD operating in a CO_2/H_2O mixture,[90] and was even more important at higher H_2O fractions in the mixture, which explains why the addition of H_2O resulted in a drop in the CO_2 conversion.[90] The situation was a bit different in our case because at higher CH_4 fractions, the H atoms formed upon dissociation of CH_4 played a more important role in the CO_2 conversion, that is, the forward (loss) reaction upon collision with H atoms was more important than the reverse reaction (production of CO_2).

The relative contributions of the net processes contributing to CH_4 conversion as a function of the CH_4 fraction in the mixture is shown in Figure 7b. The reaction of CH_4 with OH radicals was by far the most important, with a contribution of 75% at low CH_4 fraction, which decreased to 45% at the highest CH_4 fraction investigated because of the somewhat lower OH concentration in the mixture (cf. Figure 6a). At the same time, the reaction with C_2H_3 radicals became gradually more important as the density of these radicals increased with increasing CH_4 fraction (cf. Figure 6b). Furthermore, the reaction of CH_4 with H or O atoms or C_3H_5 radicals also played a minor role, as indicated in Figure 7b. The C_2H_3 and C_3H_5 radicals, as well as the H atoms, originated from CH_4. The H atoms were mainly formed by CH_4 dissociation into radicals, whereas the C_2H_3 and C_3H_5 radicals were mainly formed inside the arc from CH_2 radicals (created by electron impact dissociation of CH_4) through the following pathways:

$CH_2 + CH_2 \rightarrow C_2H_4$; $C_2H_4 + H \rightarrow C_2H_3 + H_2$
$CH_2 + CH_2 \rightarrow C_2H_2 + 2H$; $C_2H_2 + CH_3 \rightarrow C_3H_5$
$C_3H_5 + H + M \rightarrow C_3H_6 + M$; $C_3H_6 \rightarrow C_2H_3 + CH_3$

Furthermore, in the region near the arc, the following pathways also contributed to the formation of C_2H_3 and C_3H_5 radicals:

$CH_3 + CH_3 \rightarrow C_2H_5 + H$; $C_2H_5 + M \rightarrow C_2H_4 + H + M$;
$C_2H_4 + H \rightarrow C_2H_3 + H_2$
$C_2H_5 + CH_3 \rightarrow C_3H_8 \rightarrow C_3H_7 + H$; $C_3H_7 \rightarrow C_3H_6 + H$;
$C_3H_6 \rightarrow C_3H_5 + H$

This helps to explain why a higher the CH_4 fraction in the mixture leads to a higher effective CH_4 conversion (Figure 1b), and thus a higher density of the C_2H_3 and C_3H_5 radicals (Figure 6b), and a larger contribution of these radicals to the CH_4 conversion, as can be deduced from Figure 7b.

Finally, the net CH_4 loss rate increased upon increasing the CH_4 fraction (Figure S7). This was mainly due to the increasing CH_4 density in the mixture and explains why the measured effective CH_4 conversion increased upon increasing CH_4 fraction (cf. Figure 1b). However, the absolute CH_4 conversion dropped (cf. Figure 1a), which was mainly attributed to the major loss process, that is, the reaction of CH_4 with OH radicals, which becomes gradually less important at higher CH_4 fraction in the mixture.

Conclusions

We have investigated the dry reforming of methane (DRM) in a gliding arc plasmatron for different CH_4 fractions in the mixture by a combination of experiments and chemical kinetics modeling. The CO_2 and CH_4 conversions reached their highest values of approximately 18 and 10%, respectively, at 25% CH_4 in the gas mixture, which corresponded to an overall energy cost of 10 kJ L^{-1} (or 2.5 eV per molecule) and an energy effi-

ciency as high as 66%. The latter was above the required energy efficiency target reported in literature to be competitive with classical thermal DRM (i.e., 60%).[2] CO and H_2 were the major products, with some smaller fractions of C_2H_x compounds formed, as well as H_2O, which could not be quantified by GC.

A very good agreement was observed between the measured and calculated conversions and energy efficiency, so the model could be used to elucidate the underlying chemical processes. The model revealed that, besides the conversion inside the arc plasma column, some (thermal) conversion of CO_2 and CH_4 also occurred in the area around the arc column, which was characterized by a relatively high temperature. Inside the arc column, the electron temperature was much higher than the gas temperature, which indicated the non-equilibrium character of the plasma and explained the good energy efficiency of this process. Indeed, the electrons activated the gas molecules by electron impact excitation, ionization, and dissociation, which created reactive species that could more easily form new molecules. The model also demonstrated the important role of the CO_2 vibrational levels. Indeed, most of the CO_2 conversion occurred upon reaction of the CO_2 vibrational levels with radicals from the plasma. However, the vibrational distribution function was in thermal equilibrium with the gas temperature. A higher energy efficiency would still be possible if the higher vibrational levels of CO_2 could be overpopulated, for example, by operating at low temperatures (in combination with high electric power) or lower pressure.

The CO_2 conversion clearly increased upon increasing CH_4 fraction in the mixture, which was explained by the model owing to the reaction of CO_2 (mainly in vibrationally excited levels) with H atoms, formed upon dissociation of CH_4. The main process responsible for CH_4 conversion was the reaction with OH radicals. Furthermore, reactions with other radicals such as C_2H_3, H, O, and C_3H_5, also played a non-negligible role in the CH_4 conversion.

Our results demonstrate that the gliding arc plasmatron is very promising for DRM, also in comparison with other plasma types, certainly when considering the energy efficiency (or energy cost). However, the conversion needs to be further improved. To date, the conversion has been limited by the fraction of gas that passes through the plasma column. Indeed, the conversion inside the arc plasma column itself was between 51 and 81% for CO_2 and was already 100% for CH_4; however, a significant fraction of the gas (ca. 85%) does not pass through the plasma column, therefore lowering the overall conversion in the GAP. We should be able to enhance the gas fraction treated by the arc by modifying the reactor design (i.e., anode and cathode configuration), enabling the arc to be developed and extended in a larger region of the reactor, or by modifying the gas inlet configuration, enabling a larger gas fraction to pass through the arc. To realize such modifications, more insight is needed in the gas flow dynamics, which is beyond the scope of the present 0D chemical kinetics model. We are currently investigating the gas flow dynamics by 2D and 3D fluid dynamics modeling[80,81] and will elaborate on these results in the future by particle tracing simulations.

Finally, the current experiments were limited to a maximum CH_4 fraction of 25%, which is well below a stoichiometric mixture of DRM. Higher CH_4 fractions yielded an unstable plasma owing to limitations of the power supply, which was designed for the GAP in pure CO_2. In the future, we would like to perform experiments for larger CH_4 fractions corresponding to a stoichiometric mixture of DRM, in which we expect higher conversions based on the trend of our current results. The latter would also be necessary if the formed CO/H_2 mixture is further used as a feed gas for methanol synthesis or for the FT synthesis of hydrocarbons.

Experimental Section

Description of the experiments

Figure 8 shows the experimental setup. The GAP consisted of two cylindrical electrodes made of stainless steel (316). The cathode formed the reactor body, whereas the reactor outlet was at the anode potential (Figure 9). The cathode had a diameter of 17.50 mm and a length of 10.20 mm, whereas the length and di-

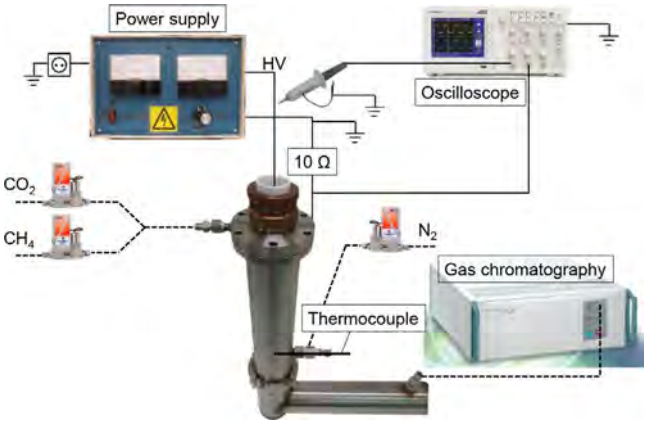

Figure 8. Schematic diagram of the experimental setup.

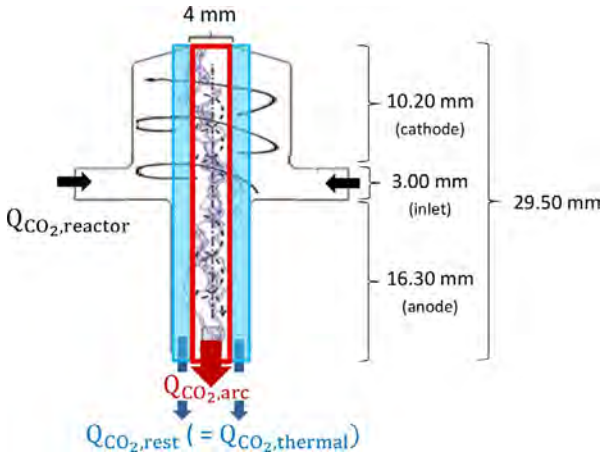

Figure 9. Schematic diagram of the GAP showing the dimensions and the outer vortex (solid spiral) and inner (reverse) vortex (dashed spiral). The red frame indicates the arc plasma column, whereas the blue part indicates the region in which thermal conversion takes place.

ameter of the anode were 16.30 and 7.08 mm, respectively. In addition, the inlet region had a width of 3 mm. This yielded a reactor volume of 3.82 cm^3. The setup can be used with different anode diameters, but the present configuration yielded the most pronounced reverse vortex flow, as revealed by computational fluid dynamics simulations, and provided the best CO_2 conversion and energy efficiency.[9]

A high voltage was applied to the GAP by means of a direct current power source. The voltage was measured by a high-voltage probe (Tektronix P6015A). The current was obtained by measuring the voltage over a 10 Ω resistor with a 10× probe. All electrical signals were recorded by a digital oscilloscope with two channels (Tektronix TDS2012C). The current and voltage inside the GAP were 0.27–0.33 A and 0.8–1.0 kV, respectively. The plasma power was calculated from the product of the plasma voltage and current over a certain time.

The gas flowed into the reactor through six tangential inlets, each with a diameter of 1.6 mm, giving rise to a vortex flow profile. The experiments were performed with a total gas flow rate of 10 L min^{-1} controlled by thermal mass flow controllers (Bronkhorst), and different fractions of CH_4 in the mixture (i.e., 0, 5, 10, 15, 20, and 25%). The outlet of the GAP was connected to a tube in which a thermocouple was used to measure the temperature of the outlet gas. The gas was further analyzed in a gas chromatograph. All experiments were performed in triplicate. Details on the gas analysis, including more information on the gas chromatograph, how to correct for gas expansion, the formulas to calculate the CO_2 and CH_4 conversion, the product selectivities, energy efficiency, and energy cost, are provided in the Supporting Information.

Description of the chemical kinetics model

The model presented herein is a 0D chemical kinetics model, called ZDPlasKin.[91] It solves the continuity equations for the various plasma species densities, based on production and loss rates [Eq. (2)]:

$$\frac{dn_i}{dt} = \sum_j \left[\left(a_{ij}^R - a_{ij}^L \right) k_j \prod_l n_l^L \right] \quad (2)$$

n_i is the density of species i, a_{ij}^R and a_{ij}^L are the stoichiometric coefficients of the species i on the left and right hand side of the reaction j, respectively. n_l is the density of the species l on the left side of the reaction, and k_j is the reaction rate coefficient of reaction j. Reaction j can be expressed in the following general form [Eq. (3)]:

$$a_A A + a_B B\ (+\delta\varepsilon) \xrightarrow{k_j} a_C C + a_D D\ (+\delta\varepsilon) \quad (3)$$

A, B, C, D are the various species, and a_A, a_B, a_C, and a_D are their stoichiometric coefficients. $\delta\varepsilon$ represents the energy needed or released by the reaction. More details about the model can be found in the Supporting Information.

In principle, ZDPlasKin can also be used to calculate the gas temperature by a heat conservation equation. However, in this work, we applied a certain temperature profile as input in the model starting from room temperature at the inlet of the arc column up to 3500 K. This was based on reported 3D fluid dynamics simulations[80,81] and experimental values.[82]

134 different plasma species, including 20 neutral molecules, 37 charged species (i.e., positive and negative ions as well as the electrons), 24 radicals, and 53 excited species, were included in the model. A complete list of these species is provided in Table S1. These species interacted with each other through various chemical reactions, including: electron impact reactions; electron–ion recombination reactions; ion–ion, ion–neutral, and neutral–neutral reactions; vibrational–translation (VT) relaxations; and (v) vibrational–vibrational (VV) relaxations.

Application of the 0D model to the GAP

The model was applied to the GAP reactor used for the experiments by considering exactly the same dimensions and operating conditions (gas flow rate of 10 L min^{-1}; CH_4 fractions in the mixture ranging from 0% to 25%; plasma power of 500 W corresponding to an SEI of 0.75 eV per molecule). A schematic diagram of the GAP including the dimensions is presented in Figure 9. The arc plasma column inside the GAP is illustrated by the red rectangle. Because the gas entered the GAP reactor through tangential inlets, it followed a vortex flow pattern. As the outlet (anode) diameter was smaller than the reactor body (cathode part) (Figure 9), the gas first moved upwards in a so-called forward vortex flow (indicated in Figure 9 by the solid spiral) and when it arrived at the top of the reactor it had lost some speed by friction and inertia and travelled downwards in a smaller so-called reverse vortex flow, which was more or less captured by the arc column (see dashed spiral in Figure 9). This vortex flow resulted in stabilization of the arc column in the center of the GAP reactor, as predicted by 3D fluid dynamics modeling.[80,81] Because the plasma confined in the inner vortex gas flow was more or less uniform,[80,81] we assumed a constant power density applied to the gas during its residence time in the plasma column. Hence, 0D modeling of this kind of plasma was justified. Indeed, the 0D model can be used to calculate the densities of the species as a function of time, and spatial variation by means of transport was not considered. Nevertheless, by means of the gas flow rate, we could convert the temporal variation calculated by the model into a spatial variation in the arc plasma column, and vice versa. The arc plasma column was considered as a plug flow reactor, in which the plasma characteristics vary as a function of distance travelled by the gas within a certain residence time, in the same way as they would vary as a function of time in a batch reactor.

Calculation of the total CO_2 and CH_4 conversion in the GAP

We calculated the conversion of CO_2 (as well as that of CH_4) after passing through the arc column with the following formula [Eq. (4)]:

$$\chi_{CO_2,arc}(\%) = \left(1 - \frac{n_{CO_2,e} \times v_e}{n_{CO_2,i} \times v_i}\right) \times 100\ \% \quad (4)$$

n_{CO_2} is the CO_2 density (in m^{-3}) and v is the gas velocity (in m s^{-1}). The indices i and e stand for the values at the beginning of the arc (i.e., room temperature) and at the end of the arc (fixed at 3500 K). Because the arc does not fill the entire GAP reactor volume (Figure 9), not all the gas was converted by the arc. Hence, to calculate the overall conversion, we multiplied the conversion by the fraction of gas that passes through the arc column, as determined by the fluxes (Supporting Information). This yielded a fraction of 14.8% of the gas that passes through the arc. However, the remaining 85.2% could still be converted thermally in the area around the arc column, which was still characterized by a high temperature (i.e., up to 2700 K; see Figure 4a). The conversion in the thermal part ($\chi_{CO_2,thermal}$) was calculated with a similar formula as Formula (4). The total CO_2 conversion was the sum of the con-

version inside the arc column ($\chi_{CO_2,arc} \times 14.8\%$) and the thermal conversion in the area around the arc column ($\chi_{CO_2,thermal} \times 85.2\%$). The same calculations were applied to the CH_4 conversion. The energy efficiency was determined from the total CO_2 and CH_4 conversion in the same way as in the experiments (see the Supporting Information, Formula 9).

Acknowledgements

We acknowledge financial support from the Fund for Scientific Research—Flanders (FWO; Grant no. G.0383.16 N) and the IAP/7 (Inter-university Attraction Pole) program "PSI-Physical Chemistry of Plasma-Surface Interactions" by the Belgian Federal Office for Science Policy (BELSPO). The calculations were performed using the Turing HPC infrastructure at the CalcUA core facility of the Universiteit Antwerpen, a division of the Flemish Supercomputer Center VSC, funded by the Hercules Foundation, the Flemish Government (department EWI), and the Universiteit Antwerpen. Finally, we would like to thank Georgi Trenchev for the 3D fluid modeling results used as input in the model, and for the assistance in the experiments.

Conflict of interest

The authors declare no conflict of interest.

Keywords: CO_2 conversion · dry reforming · hydrogen · kinetics · plasma chemistry

[1] A. Fridman, *Plasma Chemistry*, Cambridge University Press, New York, **2008**.
[2] R. Snoeckx, A. Bogaerts, *Chem. Soc. Rev.*, in press.
[3] A. Bogaerts, E. Neyts, R. Gijbels, J. van der Mullen, *Spectrochim. Acta Part B* **2002**, *57*, 609 – 658.
[4] A. Fridman, A. Chirokov, A. Gutsol, *J. Phys. D Appl. Phys.* **2005**, *38*, R1 – R24.
[5] S. R. Sun, H. X. Wang, D. H. Mei, X. Tu, A. Bogaerts, *J. CO2 Util.* **2017**, *17*, 220 – 234.
[6] I. Rusu, J. M. Cormier, *Chem. Eng. J.* **2003**, *91*, 23 – 31.
[7] F. Ouni, A. Khacef, J. M. Cormier, *Chem. Eng. Technol.* **2006**, *29*, 604 – 609.
[8] T. Nunnally, K. Gutsol, A. Rabinovich, A. Fridman, A. Gutsol, A. Kemoun, *J. Phys. D* **2011**, *44*, 274009.
[9] M. Ramakers, G. Trenchev, S. Heijkers, W. Wang, A. Bogaerts, *ChemSusChem* **2017**, *10*, 2642 – 2652.
[10] J. L. Liu, H. W. Park, W. J. Chung, D. W. Park, *Plasma Chem. Plasma Process.* **2016**, *36*, 437 – 449.
[11] A. Wu, J. Yan, H. Zhang, M. Zhang, C. Du, X. Li, *Int. J. Hydrogen Energy* **2014**, *39*, 17656 – 17670.
[12] Z. A. Allah, J. C. Whitehead, *Catal. Today* **2015**, *256*, 76 – 79.
[13] J. L. Liu, H. W. Park, W. J. Chung, W. S. Ahn, D. W. Park, *Chem. Eng. J.* **2016**, *285*, 243 – 251.
[14] K. Li, J. L. Liu, X. Li, X. Zhu, A. Zhu, *Chem. Eng. J.* **2016**, *288*, 671 – 679.
[15] Y. N. Chun, H. W. Song, S. C. Kim, M. S. Lim, *Energy Fuels* **2008**, *22*, 123 – 127.
[16] R. Snoeckx, R. Aerts, X. Tu, A. Bogaerts, *J. Phys. Chem. C* **2013**, *117*, 4957 – 4970.
[17] R. Snoeckx, Y. X. Zeng, X. Tu, A. Bogaerts, *RSC Adv.* **2015**, *5*, 29799 – 29808.
[18] X. Tu, J. C. Whitehead, *Appl. Catal. B* **2012**, *125*, 439 – 448.
[19] A. Ozkan, T. Dufour, G. Arnoult, P. De Keyzer, A. Bogaerts, F. Reniers, *J. CO2 Util.* **2015**, *9*, 74 – 81.
[20] V. Goujard, J.-M. Tatibouët, C. Batiot-Dupeyrat, *Appl. Catal. A* **2009**, *353*, 228 – 235.
[21] X. Zhang, M. S. Cha, *J. Phys. D* **2013**, *46*, 415205.
[22] Q. Wang, B. H. Yan, Y. Jin, Y. Cheng, *Plasma Chem. Plasma Process.* **2009**, *29*, 217 – 228.
[23] H. K. Song, J. W. Choi, S. H. Yue, H. Lee, B. K. Na, *Catal. Today* **2004**, *89*, 27 – 33.
[24] A. Zhang, A. Zhu, J. Guo, Y. Xu, C. Shi, *Chem. Eng. J.* **2010**, *156*, 601 – 606.
[25] Y. Li, C. J. Liu, B. Eliasson, Y. Wang, *Energy Fuels* **2002**, *16*, 864 – 870.
[26] Y. Zhang, Y. Li, Y. Wang, C. Liu, B. Eliasson, *Fuel Process. Technol.* **2003**, *83*, 101 – 109.
[27] N. R. Pinhão, a. Janeco, J. B. Branco, *Plasma Chem. Plasma Process.* **2011**, *31*, 427 – 439.
[28] H. Song, H. Lee, J.-W. Choi, B. Na, *Plasma Chem. Plasma Process.* **2004**, *24*, 57 – 72.
[29] W. Chung, K. Pan, H. Lee, M. Chang, *Energy Fuels* **2014**, *28*, 7621 – 7631.
[30] Y. Zeng, X. Zhu, D. Mei, B. Ashford, X. Tu, *Catal. Today* **2015**, *256*, 80 – 87.
[31] Q. Wang, Y. Cheng, Y. Jin, *Catal. Today* **2009**, *148*, 275 – 282.
[32] S. Mahammadunnisa, P. M. K. Reddy, B. Ramaraju, C. Subrahmanyam, *Energy Fuels* **2013**, *27*, 4441 – 4447.
[33] X. Zheng, S. Tan, L. Dong, S. Li, H. Chen, *J. Power Sources* **2015**, *274*, 286 – 294.
[34] D. Mei, X. Zhu, C. Wu, B. Ashford, P. T. Williams, X. Tu, *Appl. Catal. B* **2016**, *182*, 525 – 532.
[35] Q. Wang, B. H. Yan, Y. Jin, Y. Cheng, *Energy Fuels* **2009**, *23*, 4196 – 4201.
[36] X. Tu, H. J. Gallon, M. V. Twigg, P. A. Gorry, J. C. Whitehead, *J. Phys. D* **2011**, *44*, 274007.
[37] X. Zheng, S. Tan, L. Dong, S. Li, H. Chen, *Int. J. Hydrogen Energy* **2014**, *39*, 11360 – 11367.
[38] K. Zhang, T. Mukhriza, X. Liu, P. P. Greco, E. Chiremba, *Appl. Catal. A* **2015**, *502*, 138 – 149.
[39] M. H. Pham, V. Goujard, J. M. Tatibouët, C. Batiot-Dupeyrat, *Catal. Today* **2011**, *171*, 67 – 71.
[40] J. Sentek, K. Krawczyk, M. Młotek, M. Kalczewska, T. Kroker, T. Kolb, A. Schenk, K. H. Gericke, K. Schmidt-Szałowski, *Appl. Catal. B* **2010**, *94*, 19 – 26.
[41] K. Krawczyk, M. Młotek, B. Ulejczyk, *Fuel* **2014**, *117*, 608 – 617.
[42] H. J. Gallon, X. Tu, J. C. Whitehead, *Plasma Processes Polym.* **2012**, *9*, 90 – 97.
[43] B. Eliasson, C. Liu, U. Kogelschatz, *Ind. Eng. Chem. Res.* **2000**, *39*, 1221 – 1227.
[44] J. J. Zou, Y. P. Zhang, C. J. Liu, Y. Li, B. Eliasson, *Plasma Chem. Plasma Process.* **2003**, *23*, 69 – 82.
[45] G. J. van Rooij, D. C. M. van den Bekerom, N. den Harder, T. Minea, G. Berden, W. A. Bongers, R. Engeln, M. F. Graswinckel, E. Zoethout, M. C. M. van de Sanden, *Faraday Discuss.* **2015**, *183*, 233 – 248.
[46] W. Bongers, H. Bouwmeester, B. Wolf, F. Peeters, S. Welzel, D. van den Bekerom, N. den Harder, A. Goede, M. Graswinckel, P. W. Groen, et al., *Plasma Process. Polym.* **2017**, *14*, e1600126.
[47] J. Q. Zhang, Y. J. Yang, J. S. Zhang, Q. Liu, *Acta Chim. Sinica* **2002**, *60*, 1973 – 1980.
[48] W. Cho, W. S. Ju, S. H. Lee, Y. S. Baek, Y. C. Kim in *Proceedings of 7th International Conference on Carbon Dioxide Utilization* **2004**, pp. 205 – 208.
[49] Z. Bo, J. Yan, X. Li, Y. Chi, K. Cen, *Int. J. Hydrogen Energy* **2008**, *33*, 5545 – 5553.
[50] X. Tu, J. C. Whitehead, *Int. J. Hydrogen Energy* **2014**, *39*, 9658 – 9669.
[51] A. Indarto, J. W. Choi, H. Lee, H. K. Song, *Energy* **2006**, *31*, 2986 – 2995.
[52] N. Rueangjitt, C. Akarawitoo, T. Sreethawong, S. Chavadej, *Plasma Chem. Plasma Process.* **2007**, *27*, 559 – 576.
[53] N. Rueangjitt, T. Sreethawong, S. Chavadej, *Plasma Chem. Plasma Process.* **2008**, *28*, 49 – 67.
[54] Y. N. Chun, Y. C. Yang, K. Yoshikawa, *Catal. Today* **2009**, *148*, 283 – 289.
[55] M. Li, C. Liu, Y. Tian, G. Xu, F. Zhang, Y. Wang, *Energy Fuels* **2006**, *20*, 1033 – 1038.
[56] A. Aziznia, H. R. Bozorgzadeh, N. Seyed-matin, M. Baghalha, A. Mohamadalizadeh, *J. Nat. Gas Chem.* **2012**, *21*, 466 – 475.
[57] M. Li, G. Xu, Y. Tian, L. Chen, H. Fu, *J. Phys. Chem. A* **2004**, *108*, 1687 – 1693.
[58] N. Seyed-Matin, A. H. Jalili, M. H. Jenab, S. M. Zekordi, A. Afzali, C. Rasouli, A. Zamaniyan, *Plasma Chem. Plasma Process.* **2010**, *30*, 333 – 347.
[59] M. A. Malik, X. Z. Jiang, *Plasma Chem. Plasma Process.* **1999**, *19*, 505 – 512.

[60] S. L. Yao, M. Okumoto, A. Nakayama, E. Suzuki, *Energy Fuels* **2001**, *15*, 1295 – 1299.
[61] Y. Yang, *Ind. Eng. Chem. Res.* **2002**, *41*, 5918 – 5926.
[62] C. J. Liu, R. G. Mallinson, L. L. Lobban, *Appl. Catal. A* **1999**, *178*, 17 – 27.
[63] W. Chung, M. Chang, *Energy Convers. Manage.* **2016**, *124*, 305 – 314.
[64] M. M. Moshrefi, F. Rashidi, H. R. Bozorgzadeh, M. Ehtemam Haghighi, *Plasma Chem. Plasma Process.* **2013**, *33*, 453 – 466.
[65] V. Shapoval, E. Marotta, *Plasma Processes Polym.* **2015**, *12*, 808 – 816.
[66] B. Zhu, X. Li, J. Liu, X. Zhu, A. Zhu, *Chem. Eng. J.* **2015**, *264*, 445 – 452.
[67] X. S. Li, B. Zhu, C. Shi, Y. Xu, A. M. Zhu, *AIChE J.* **2011**, *57*, 2854 – 2860.
[68] S. Kado, K. Urasaki, Y. Sekine, K. Fujimoto, *Fuel* **2003**, *82*, 1377 – 1385.
[69] B. Zhu, X. S. Li, C. Shi, J. L. Liu, T. L. Zhao, A. M. Zhu, *Int. J. Hydrogen Energy* **2012**, *37*, 4945 – 4954.
[70] K. Li, J. Liu, X. Li, X. Zhu, A. Zhu, *Catal. Today* **2015**, *256*, 96 – 101.
[71] A. Huang, G. Xia, J. Wang, S. L. Suib, Y. Hayashi, H. Matsumoto, *J. Catal.* **2000**, *189*, 349 – 359.
[72] D. Li, X. Li, M. Bai, X. Tao, S. Shang, X. Dai, Y. Yin, *Int. J. Hydrogen Energy* **2009**, *34*, 308 – 313.
[73] H. Long, S. Shang, X. Tao, Y. Yin, X. Dai, *Int. J. Hydrogen Energy* **2008**, *33*, 5510 – 5515.
[74] M. Scapinello, L. M. Martini, G. Dilecce, P. Tosi, *J. Phys. D* **2016**, *49*, 075602.
[75] A. M. Ghorbanzadeh, S. Norouzi, T. Mohammadi, *J. Phys. D* **2005**, *38*, 3804 – 3811.
[76] S. L. Yao, F. Ouyang, A. Nakayama, E. Suzuki, M. Okumoto, A. Mizuno, *Energy Fuels* **2000**, *14*, 910 – 914.
[77] B. Dai, X. L. Zhang, W. M. Gong, R. He, *Plasma Sources Sci. Technol.* **2000**, *9*, 577 – 580.
[78] A. M. Ghorbanzadeh, R. Lotfalipour, S. Rezaei, *Int. J. Hydrogen Energy* **2009**, *34*, 293 – 298.
[79] X. Zhang, B. Dai, A. Zhu, W. Gong, C. Liu, *Catal. Today* **2002**, *72*, 223 – 227.
[80] G. Trenchev, S. Kolev, A. Bogaerts, *Plasma Sources Sci. Technol.* **2016**, *25*, 035014.
[81] G. Trenchev, St. Kolev, W. Wang, M. Ramakers, A. Bogaerts, *J. CO2 Utiliz.* (submitted).
[82] T. Nunnally, *Application of Low Current Gliding Arc Plasma Discharges for Hydrogen Sulfide Decomposition and Carbon Dioxide Emission Reduction*, Drexel University, **2011**.
[83] W. Wang, A. Berthelot, S. Kolev, X. Tu, A. Bogaerts, *Plasma Sources Sci. Technol.* **2016**, *25*, 065012.
[84] W. Wang, D. Mei, X. Tu, A. Bogaerts, *Chem. Eng. J.* (in press).
[85] S. Heijkers, A. Bogaerts, *J. Phys. Chem. C* (submitted).
[86] A. Berthelot, A. Bogaerts, *J. Phys. Chem. C* **2017**, *121*, 8236 – 8251.
[87] S. Heijkers, R. Snoeckx, T. Kozák, T. Silva, T. Godfroid, N. Britun, R. Snyders, A. Bogaerts, *J. Phys. Chem. C* **2015**, *119*, 12815 – 12828.
[88] T. Kozák, A. Bogaerts, *Plasma Sources Sci. Technol.* **2014**, *23*, 045004.
[89] A. Berthelot, A. Bogaerts, *Plasma Sources Sci. Technol.* **2016**, *25*, 045022.
[90] R. Snoeckx, A. Ozkan, F. Reniers, A. Bogaerts, *ChemSusChem* **2017**, *10*, 409 – 424.
[91] S. Pancheshnyi, B. Eismann, G. J. M. Hagelaar, L. C. Pitchford, *Computer code ZDPlasKin*, http://www.zdplaskin.laplace.univ-tlse.fr (University of Toulouse, LAPLACE, CNRS-UPS-INP, Toulouse, France, **2008**).

Manuscript received: July 13, 2017
Revised manuscript received: August 18, 2017
Accepted manuscript online: August 22, 2017
Version of record online: October 2, 2017

CHEMISTRY & SUSTAINABILITY
CHEMSUSCHEM
ENERGY & MATERIALS

Supporting Information

Dry Reforming of Methane in a Gliding Arc Plasmatron: Towards a Better Understanding of the Plasma Chemistry

Emelie Cleiren, Stijn Heijkers, Marleen Ramakers,* and Annemie Bogaerts*[a]

cssc_201701274_sm_miscellaneous_information.pdf

Details on the experiments

Gas analysis

The gas chromatograph used is a compact gas chromatograph (CGC) of Interscience. One measurement takes only 400 s, which is much shorter than for classical GCs. The CGC is equipped with three different ovens, each with a separate column and detector. The first channel has a Rtx-1 column and a flame ionization detector (FID), which can be used to measure alkanes, alkenes and alkynes. The other two channels make use of thermal conductivity detectors (TCDs). The middle channel has two columns, a molecular sieve (Molsieve 5A) and a RT-QBond, and the TCD measures the permanent gases, like O_2, N_2, CO, H_2 and CH_4. The last channel has two RT-QBond columns, which allow the separation of CO_2, lower hydrocarbons (up to C_3), alcohols, aldehydes and ketones.

First a calibration is performed for the compounds to be detected, namely CO_2, CO, O_2, CH_4, H_2, C_2H_2, C_2H_4 and C_2H_6. C_2H_2 and C_2H_4 cannot be separated with the CGC. However, because of their low concentrations (see also Figure 6(b) in the main paper), the C_2-compounds (C_2H_n ; n = 2, 4 or 6) are considered as one compound. H_2O is detected as a broad band, which cannot be quantified. Higher hydrocarbons and oxygenated compounds cannot be detected with this CGC.

Determination of the CO_2 and CH_4 conversion

By analyzing the gas mixture with and without plasma, we can calculate the CO_2 and CH_4 conversions by Formula (1). $C_{i\,(\mathrm{in})}$ and $C_{i\,(\mathrm{out})}$ are the concentrations of component *i* (CO_2 or CH_4) measured after passing through the GAP without plasma (blank measurement) and with plasma, respectively. α is a correction factor, explained in the next section.

$$\chi_i(\%) = \frac{C_{i\,(\mathrm{in})} - \alpha \cdot C_{i\,(\mathrm{out})}}{C_{i(\mathrm{in})}} \cdot 100\ \% \qquad i = CO_2 \text{ or } CH_4 \qquad (1)$$

Besides this (absolute) conversion, we also determine the effective conversion for both CO_2 and CH_4, accounting for the fraction of this component present in the initial gas mixture:

$$\chi_{\mathrm{eff},i}(\%) = \chi_i(\%) \cdot \mathrm{fraction}_i \qquad i = CO_2 \text{ or } CH_4 \qquad (2)$$

The total conversion is the sum of both effective conversions, and is of interest to compare mixtures with different CO_2/CH_4 ratios.

Correction factor for the gas expansion

The correction factor 'α' in Formula (1) accounts for gas expansion taking place during the reaction. Indeed, both in pure CO_2 splitting and dry reforming of methane (DRM), the number of molecules rises during reaction, so the volumetric flux will rise as well. Because the GC always samples the same volume of the gas flow, neglecting this correction factor, which is done in most papers on plasma-based gas conversion, would overestimate the conversion.[1] Indeed, the sample loop of the GC has a fixed volume, so that gas expansion will yield a pressure rise. However, the GC always samples at atmospheric pressure, so part of the gas will be lost before being injected in the GC. Hence, the number of molecules that will arrive in this sample volume is lower than the original number in the outlet flow. Thus, less molecules will be measured in the sample, which manifests itself as a higher conversion.

To account for this gas expansion, we add an internal standard (N_2) to the outlet gas flow. Using an internal standard has several advantages: (i) it is easy to implement; (ii) no extra calibration is needed; (iii) it has no effect on the reaction processes; (iv) it can be used with every gas mixture.[1]

By comparing the peak surface area of N_2 in the chromatogram with and without plasma, we can obtain the correction factor α (Formula (3))[1] assuming that the ratio of the surface areas is proportional with the ratio of the fluxes.

$$\alpha = \frac{A_{N_2,\text{blank}}}{A_{N_2,\text{plasma}}}(1+\beta) - \beta \tag{3}$$

β is equal to the ratio of the gas flow rate of the internal standard with respect to the total gas flow rate in the GAP (Formula (4)). In this work we always use 10 % of the total gas flow rate as internal standard (β = 0.1), hence for a total gas flow rate of 10 L/min, we add 1 L/min N_2 as internal standard.

$$\beta = \frac{\Phi_{\text{standard}}}{\Phi_{\text{effluent}}} = \frac{\text{gas flow rate}_{N_2}}{\text{gas flow rate}_{CO_2+CH_4}} \tag{4}$$

By adding the internal standard, we need to correct the measured concentrations (C_m) by means of Formula (5) and (6), for the blank measurements and the plasma measurements, respectively.[1]

$$C^{\text{blank}} = C_m^{\text{blank}}(1+\beta) \tag{5}$$

$$C^{\text{plasma}} = C_m^{\text{plasma}}\left(1+\frac{\beta}{\alpha}\right) \tag{6}$$

In the following, we always use the corrected concentrations.

Determination of the specific energy input (SEI), energy efficiency and energy cost

The SEI is calculated from the plasma power and the gas flow rate:

$$\text{SEI (J cm}^{-3}\text{)} = \text{SEI (kJ L}^{-1}\text{)} = \frac{P_{\text{plasma}}\ (\text{kW})}{\text{gas flow rate (L min}^{-1}\text{)}} \cdot 60\ (\text{s min}^{-1}) \tag{7}$$

It can also be expressed in eV/molec:

$$\text{SEI (eV molec}^{-1}\text{)} = \frac{\text{SEI (kJ L}^{-1}\text{)} \cdot V_{\text{mol}}\ (\text{L mol}^{-1}) \cdot 10^3\left(\text{J kJ}^{-1}\right)}{1{,}6.10^{-19}\left(\text{J eV}^{-1}\right) \cdot 6{,}022.10^{23}\left(\text{molec mol}^{-1}\right)} \tag{8}$$

V_{mol} is the molar volume, being equal to 22.4 L mol^{-1} (at 0 °C and 1 atm).

The energy efficiency (η) is calculated as follows:

$$\eta = \frac{\alpha \cdot C_{CO(out)} \cdot H_{f,CO} - (\chi_{CH_4} \cdot C_{CH_{4(in)}} \cdot H_{f,CH_4} + \chi_{CO_2} \cdot C_{CO_{2(in)}} \cdot H_{f,CO_2})}{SEI\ (kJ\ L^{-1}) \cdot V_{mol}\ (L\ mol^{-1})} \quad (9)$$

H_f is the enthalpy of formation ($H_{f,CO}$= -110,5 kJ mol^{-1}; H_{f,CH_4}= -74,8 kJ mol^{-1}; H_{f,CO_2}= -393,5 kJ mol^{-1}). The SEI is converted into kJ mol^{-1} by means of the molar volume. This definition yields the chemical energy efficiency. For the sake of completeness, the enthalpy of formation of C_2H_n (n = 2, 4 of 6), and of other possible (oxygenated) compounds, should be accounted for in the numerator. However, due to the nearly negligible concentrations of these products, these terms can be neglected here.

Finally, the total energy cost (EC) is expressed as:

$$EC_{total}(eV\ molec^{-1}) = \frac{SEI\ (eV\ molec^{-1})}{\chi_{total}} \quad (10)$$

Determination of the product selectivities and carbon balance

The C-, H- and O-based selectivities of CO, the C_2-based hydrocarbons (C_2H_n ; n = 2, 4 or 6, expressed as C_2), H_2 and O_2, are calculated as follows:

$$S_{C,CO} = \frac{\alpha \cdot C_{CO(out)}}{(C_{CO_2(in)} - \alpha \cdot C_{CO_2(out)}) + (C_{CH_4(in)} - \alpha \cdot C_{CH_4(out)})} \quad (11)$$

$$S_{C,C_2} = \frac{2 \cdot \alpha \cdot C_{C_2(out)}}{(C_{CO_2(in)} - \alpha \cdot C_{CO_2(out)}) + (C_{CH_4(in)} - \alpha \cdot C_{CH_4(out)})} \quad (12)$$

$$S_{H,H_2} = \frac{\alpha \cdot C_{H_2(out)}}{2 \cdot (C_{CH_4(in)} - \alpha \cdot C_{CH_4(out)})} \quad (13)$$

$$S_{O,O_2} = \frac{\alpha \cdot C_{O_2(out)}}{C_{CO_2(in)} - \alpha \cdot C_{CO_2(out)}} \quad (14)$$

Finally, to determine the ratio of the total number of C atoms in the products vs in the reactant, we calculate the carbon balance:

$$b_C = \frac{\alpha \cdot (C_{CO(out)} + C_{CO_2(out)} + C_{CH_4(out)} + 2 \cdot C_{C_2(out)})}{C_{CO_2(in)} + C_{CH_4(out)}} \quad (15)$$

Details on the computational model

0D model ZDPlasKin

ZDPlasKin (i.e., *Zero-Dimensional Plasma Kinetics solver*)[2] is a Fortran 90 computer code developed to calculate the species densities and the gas temperature as a function of time in non-equilibrium plasmas, by means of conservation equations. The species densities are calculated by continuity equations, based on production and loss rates. A large number of chemical reactions are included. The rate coefficients k_j for reactions between heavy particles are adopted from literature, as a function of gas temperature. The rate coefficients for reactions of electrons depend on the electron energy (and thus on the electron energy distribution function - EEDF), which is defined by the electron temperature or the reduced electric field (i.e., ratio of electric field over gas density; E/n). The latter is calculated by means of a Boltzmann solver (Bolsig+[3]), integrated in ZDPlasKin. This Boltzmann solver solves the Boltzmann equation for electrons, resulting in the EEDF. To solve this equation, we need to know the cross sections of the various elastic and inelastic collisions that can affect the EEDF. These cross sections are adopted from literature.[4-6] The rate coefficients (k_j) for reactions with electrons are calculated as:

$$k_j = \int_0^{+\infty} \sigma_j(\varepsilon) f_e(\varepsilon) \sqrt{\frac{2\varepsilon}{m_e}} d\varepsilon \quad (16)$$

ε is the electron energy, $\sigma_j(\varepsilon)$ the cross section of the j-th reaction, $f_e(\varepsilon)$ the EEDF and m_e the mass of an electron (9.1094x10^{-31} kg).

The electric field (E in V.m^{-1}) is calculated by the so-called local field approximation:[7]

$$E = \sqrt{P/\sigma} \quad (17)$$

P is the power density (in W m^{-3}) and σ is the plasma (specific) conductivity (in A V^{-1} m^{-1}), which is estimated in the beginning of the simulation as follows:[7]

$$\sigma = \frac{e^2 \cdot n_{e,init}}{m_e \cdot \nu_m} \quad (18)$$

e is the charge of an electron (1.6022x10^{-19} C), $n_{e,init}$ the initial electron density (in m^{-3}), m_e the mass of an electron (cf. formula (16)) and ν_m the collision frequency (in s^{-1}). The plasma conductivity is updated during the simulations by:[7]

$$\sigma = \frac{e \cdot v_d \cdot n_e}{(E/n)_{previous} \cdot n_0} \quad (19)$$

v_d is the drift velocity of the electrons, calculated with Bolsig+, and $(E/n)_{previous}$ is the reduced electric field in the previous time step.

Finally, the power density, P, is obtained from the arc volume and the plasma power. The latter is simply obtained from the experiments (see main paper and see also Figure S.1 below). The arc volume, however, cannot easily be obtained from the experiments. Nevertheless, based on a 3D fluid plasma model, the movement of the arc in the GAP was simulated,[8] and it was revealed that the arc has a radius of about 1 mm. However, the temperature just outside the arc is still high enough to induce a plasma. Moreover, the 3D simulations were carried out for argon, and we may expect that the temperature outside the arc column is higher for a molecular plasma like CO_2, because of the vibration-translation (VT) relaxations, causing a rise in temperature. Not much is known in literature about the effect of CH_4 on these VT relaxations and the associated heating, but we can safely assume that the arc radius will be larger than 1 mm. In our simulations we assume an arc radius of 2 mm. Combined with the length of the cathode (10.20 mm) and anode (16.30 mm) and the inlet of 3 mm (see Figure 9 of the main paper), this yields a plasma volume of 0.37 cm^3.

Details of the chemistry set

The chemistry set for the conversion of CO_2 and CH_4 (i.e., dry reforming of methane, DRM*)* in our GAP is based on the chemistry set for DRM in a DBD,[6] but extended with the vibrational levels of CO_2. The latter are not included in the chemistry set of the DBD, because vibrationallly excited species have a negligible effect in a DBD, while they are crucial for the dissociation process of CO_2 in a GAP, due to the lower values of the reduced electric field.[9,10] The vibrational levels of CH_4 are limited to the first two levels, because it is known from literature that they have a much smaller population than the vibrational levels of CO_2.[10]

The various plasma species considered in the model are listed in Table S.1. The symbols 'V' and 'E' represent the vibrational and electronic excited levels of CO_2, CO, O_2, CH_4 and H_2. All 21 levels (V_1-V_{21}) of the asymmetric stretch mode of CO_2 (*00n*), up to the dissociation limit of 5.5 eV, are included, because this asymmetric vibrational mode is the most important for energy-efficient dissociation of CO_2.[10] Besides the 21 levels of the asymmetric stretch mode of CO_2, also four (combined) lower lying levels of the symmetric stretch and bending modes are included in the model. Only one electronically excited level of CO_2 (E_1), with a threshold energy of 10.5 eV, is considered, because the

other low-lying energy levels immediately give rise to dissociation. The notation, energy and identification of all excited levels is given in Table S.2.

Table S.1: Overview of the species included in the 0D model. An explanation of the notation of the excited species is given in Table S.2.

Neutral molecules	***Charged species***	***Radicals***	***Excited species***
	electrons		
CO_2, CO	CO_2^+, CO_4^+, CO^+, $C_2O_2^+$, $C_2O_3^+$, $C_2O_4^+$, C_2^+, C^+, CO_3^-, CO_4^-	C_2O, C, C_2	CO_2 (V_a, V_b, V_c, V_d), CO_2 (V_1-V_{21}), CO_2 (E_1: 10,5 eV) CO (V_1-V_{10}), CO (E_1-E_4)
O_2, O_3	O^+, O_2^+, O_4^+, O^-, O_2^- O_3^-, O_4^-	O	O_2 (V_1-V_4), O_2 (E_1-E_2)
CH_4	CH_5^+, CH_4^+, CH_3^+, CH_2^+, CH^+	CH_3, CH_2, CH	CH_4 (V_1, V_2)
C_2H_6, C_2H_4, C_2H_2	$C_2H_6^+$, $C_2H_5^+$, $C_2H_4^+$, $C_2H_3^+$, $C_2H_2^+$, C_2H^+	C_2H_5, C_2H_3, C_2H	
C_3H_8, C_3H_6		C_3H_7, C_3H_5	
H_2	H_3^+, H_2^+, H^+, H^-	H	H_2(V_1-V_3), H_2(E_1), H(^{2}P)
H_2O, H_2O_2 CH_2O, CH_3OH, CH_3OOH C_2H_5OH, C_2H_5OOH CH_3CHO, CH_2CO	H_3O^+, H_2O^+, OH^+, OH^-	OH, HO_2 CHO, CH_2OH, CH_3O, CH_3O_2 C_2HO, CH_3CO CH_2CHO, C_2H_5O, $C_2H_5O_2$	

Table S.2: Notation, corresponding energy and identification of the excited levels considered in the model and listed in Table S.1.

	Notation	***Energy (eV)***	***Identification***
Symmetric vibration modes of CO_2	CO_2 (V_a)	0.083	(0 1 0)
	CO_2 (V_b)	0.167	(0 2 0) + (1 0 0)
	CO_2 (V_c)	0.252	(0 3 0) + (1 1 0)
	CO_2 (V_d)	0.339	(0 4 0) + (1 2 0) + (2 0 0)
Asymmetric vibration modes of CO_2	CO_2 (V_1)	0.29	(0 0 1)
	CO_2 (V_2)	0.58	(0 0 2)
	CO_2 (V_3)	0.86	(0 0 3)
	CO_2 (V_4)	1.14	(0 0 4)
	CO_2 (V_5)	1.43	(0 0 5)
	CO_2 (V_6)	1.70	(0 0 6)
	CO_2 (V_7)	1.97	(0 0 7)
	CO_2 (V_8)	2.24	(0 0 8)
	CO_2 (V_9)	2.51	(0 0 9)

	CO_2 (V_{10})	2.77	(0 0 10)
	CO_2 (V_{11})	3.03	(0 0 11)
	CO_2 (V_{12})	3.29	(0 0 12)
	CO_2 (V_{13})	3.55	(0 0 13)
	CO_2 (V_{14})	3.80	(0 0 14)
	CO_2 (V_{15})	4.04	(0 0 15)
	CO_2 (V_{16})	4.29	(0 0 16)
	CO_2 (V_{17})	4.53	(0 0 17)
	CO_2 (V_{18})	4.77	(0 0 18)
	CO_2 (V_{19})	5.01	(0 0 19)
	CO_2 (V_{20})	5.24	(0 0 20)
	CO_2 (V_{21})	5.47	(0 0 21)
Electronically excited levels of CO_2	CO_2 (E_1)	10.5	$^1\Delta_u$
Vibrational levels of CO	CO (V_1)	0.266	
	CO (V_2)	0.528	
	CO (V_3)	0.787	
	CO (V_4)	1.040	
	CO (V_5)	1.300	
	CO (V_6)	1.540	
	CO (V_7)	1.790	
	CO (V_8)	2.030	
	CO (V_9)	2.270	
	CO (V_{10})	2.510	
Electronically excited levels of CO	CO (E_1)	6.22	$A^3\Pi$
	CO (E_2)	7.90	$A^1\Pi$
	CO (E_3)	10.4	$A^3\Sigma$, $D^3\Delta$, $E^3\Sigma$, $B^3\Sigma$
	CO (E_4)	10.6	$C^1\Sigma$, $E^1\Pi$, $B^1\Sigma$, $I^1\Sigma$, $D^1\Delta$
Vibrational level of O_2	O_2 (V_n)	0.19 – 0.38 – 0.57 – 0.75	n = 1,…,4
Electronically excited levels of O_2	O_2 (E_1)	0.98	$A^1\Delta$, $B^1\Sigma$
	O_2 (E_2)	8.40	$B^3\Sigma$
Vibrational levels of CH_4	CH_4 (V_n)	0.162 – 0.361	n = 1, 2
Excited levels of H_2 and H	H_2 (V_n)	0.516 – 1.0 – 1.50	n = 1, 2 ,3
	H_2 (E_1)	8.9	$B^3\Sigma$
	H (^{2}P)	10.2	

Besides the difference in the importance of the vibrational levels between a DBD and a GAP, also the temperature is greatly different. In contrast to a DBD reactor, which operates (more or less) at room temperature, the temperature in a GAP is much higher (i.e., around 3000-3500 K, according to 3D simulations for argon).[8] Thus, the temperature dependence must be accounted for in the reaction rate coefficients, compared to the DBD chemistry set of [6]. The rate coefficients, including their

temperature dependence, are adopted from the NIST database (*National Institute of Standards and Technology Chemical Kinetics Database*).[11]

Calculation of the fraction of gas passing through the arc column

The total gas conversion in the GAP is defined by the conversion inside the arc column, multiplied with the fraction of gas passing through this arc column. In addition, the fraction of gas that does not pass through the arc column, can also thermally be converted, as explained in the main paper.

The total CO_2 conversion by the arc, accounting for the limited fraction of gas passing through the arc, is calculated by:

$$\chi_{CO_2,arc}^{total}(\%) = \left(1 - \frac{Q_{CO_2,arc} + Q_{CO_2,rest}}{Q_{CO_2,reactor}}\right) \cdot 100\ \% \tag{20}$$

$Q_{CO_2,reactor}$, $Q_{CO_2,arc}$ and $Q_{CO_2,rest}$ are the particle fluxes (in s^{-1}) of CO_2 entering the GAP reactor, leaving the arc, and the flux of CO_2 molecules that do not pass through the arc, and will thus not be treated by the plasma. These fluxes are calculated as follows:

$$Q_{CO_2,reactor} = n_{CO_2,i} \cdot \dot{V} \tag{21}$$

$$Q_{CO_2,arc} = n_{CO_2,e} \cdot v_e \cdot A_{arc} \tag{22}$$

$$Q_{CO_2,rest} = Q_{CO_2,reactor} - n_{CO_2,i} \cdot v_i \cdot A_{arc} \tag{23}$$

n_{CO_2} is the CO_2 density (in m^{-3}) and v is the gas velocity (in m s^{-1}). The indices i and e stand for the values at the beginning of the arc (hence at room temperature) and at the end of the arc (fixed at 3500 K). $\dot{V}$ stands for the volumetric gas velocity (m^3 s^{-1}) and A_{arc} is the cross section of the arc column, being equal to 12.57 mm^2 (as the arc radius is 2 mm).

Inserting these fluxes in Formula (20), and using the gas velocity at the beginning of the arc, as obtained from 3D simulations (i.e., 1.96 m/s), yields:

$$\chi_{CO_2,arc}^{total}(\%) = \frac{(n_{CO_2,b} \cdot v_i - n_{CO_2,e} \cdot v_e) \cdot A_{arc}}{n_{CO_2,i} \cdot \dot{V}} \cdot 100\ \%$$

$$\Leftrightarrow$$

$$\chi_{CO_2,arc}^{total}(\%) = \chi_{CO_2,arc}(\%) \cdot \frac{v_i \cdot A_{arc}}{\dot{V}}$$

$$= \chi_{CO_2,arc}(\%) \cdot \frac{1.96\ \mathrm{m\ s^{-1}}\ \mathrm{x}\ 12.57\mathrm{x}10^{-6}\ \mathrm{m^2}}{10\ \mathrm{x}\ 10^{-3}\ \mathrm{m^3\ min^{-1}}/(60\ \mathrm{s\ min^{-1}})}$$

$$= \chi_{CO_2,arc}(\%) \cdot 0.148$$

Note that the same reasoning also applies to CH_4.

Extra information on the experimental results

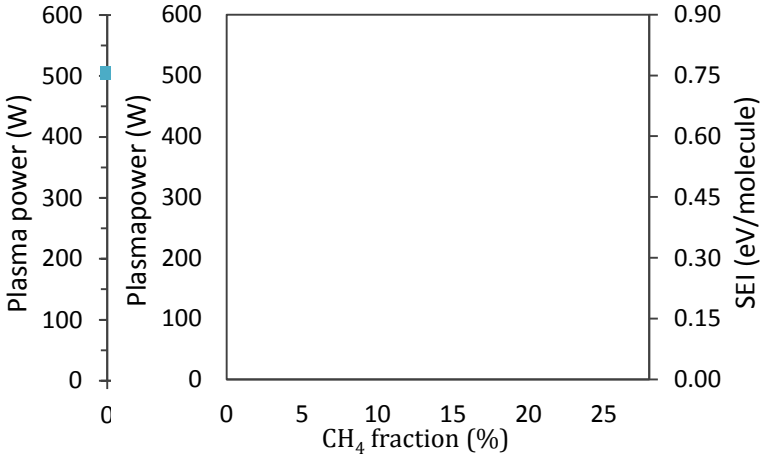

Figure S.1: Plasma power (left axis) and specific energy input (SEI; right axis) as a function of the CH_4 fraction in the mixture, showing that they are more or less constant in the entire gas mixing ratio.

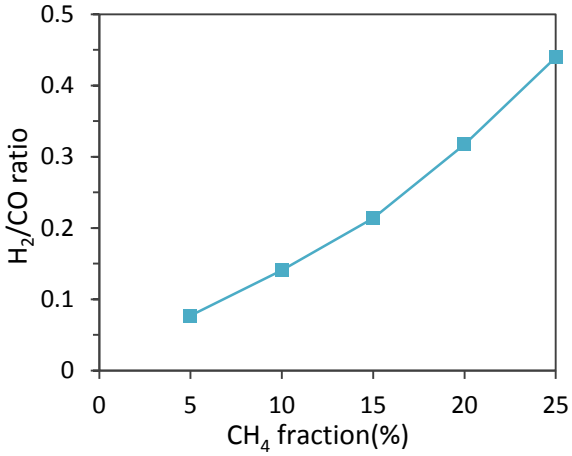

Figure S.2: H_2/CO ratio as a function of the CH_4 fraction in the mixture, showing a slightly more than linear increase.

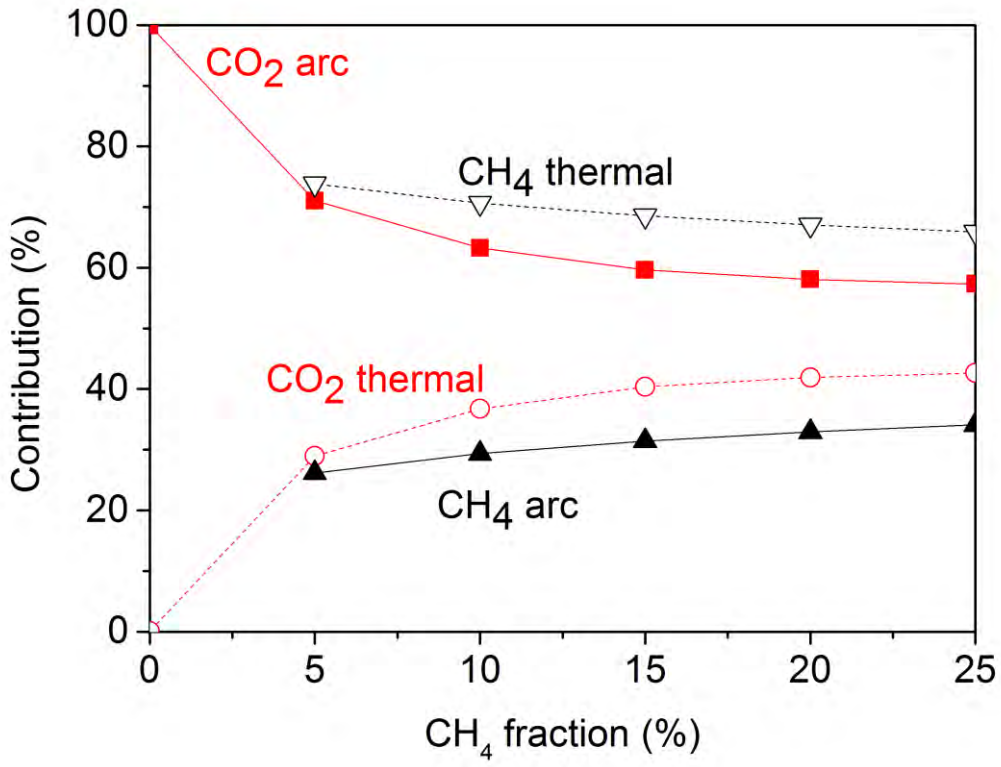

Figure S.3: Relative contribution of the conversion inside the arc and the thermal conversion in the area around the arc to the overall conversion of CO_2 and CH_4, as a function of the CH_4 fraction in the mixture.

Extra information on the calculation results: Detailed analysis of the loss and formation processes of CO_2 and CH_4

Loss and formation of CO_2

Figure S.4 illustrates the time-integrated rates of the major loss (a) and formation (b) processes of CO_2, as a function of the CH_4 fraction in the mixture. The solid lines represent contributions from the vibrationally excited levels of CO_2, while the dashed lines (in the same color) indicate the same reactions from the ground state. It is clear from Figure S.4(a) that the reactions from the CO_2 vibrational levels are more important than those from the ground state, and that the reaction with H atoms (mainly from the vibrational levels, i.e., $CO_2(v) + H \rightarrow CO + OH$; black curve) is by far the dominant loss process. The reactions of $CO_2(v)$ with O atoms or any molecule M (red and blue curve) are only important at low CH_4 fractions, where the H atom density is still low, and the O atom density is still high (cf. also Figure 6(a) from the main paper). Indeed, in the CO_2/CH_4 mixture, the O atoms will react with CH_4 (and dissociation products, like H atoms), to form OH (and CH_3) radicals, so their contribution in CO_2 splitting drops.

In spite of the fact that the reaction of CO_2 with H atoms is by far the dominant one, its opposite reaction (i.e., $CO + OH \rightarrow CO_2 + H$) is nearly equally important, as shown in Figure S.4(b). The same applies, to a lower extent, for the opposite reactions of the collisions with O atoms or molecules M (cf. red and blue curves in Figures S.4(b)). Therefore, we need to look at the time-integrated rates of the net reactions (i.e., forward minus reverse reaction of the same kind) and they are plotted in Figure S.5. The same colors are used as in Figure S.4, for the sake of clarity. Furthermore, the total (time-integrated) net loss rate is also plotted. Note that the rates of the net loss reactions are plotted

as negative values, while the net production reaction rates would occur as positive values. It is, however, clear from Figure S.5 that there is a net loss of CO_2, for all gas mixing ratios investigated, and the loss rate rises with increasing CH_4 fraction in the mixture. This explains the higher CO_2 conversion upon higher CH_4 fraction in the mixture. The reaction of CO_2 with H atoms is the most important net loss process, except at low CH_4 fractions, where reactions with O atoms or molecules M are more important, but their contribution drops upon rising CH_4 fraction. The fact that the net rate of the reaction with O atoms rises at 5 % CH_4 fraction is because the rate of the opposite reaction ($CO + O_2 \rightarrow CO_2 + O$) drops faster than the rate of the forward reaction ($CO_2 + O \rightarrow CO + O_2$) upon addition of CH_4. However, at larger CH_4 fractions, the rate of the forward reaction also drops due to the lower O atom density in the plasma. Finally, the contribution of electron impact dissociation is not negligible, and seems to be independent from the CH_4 fraction in the mixture.

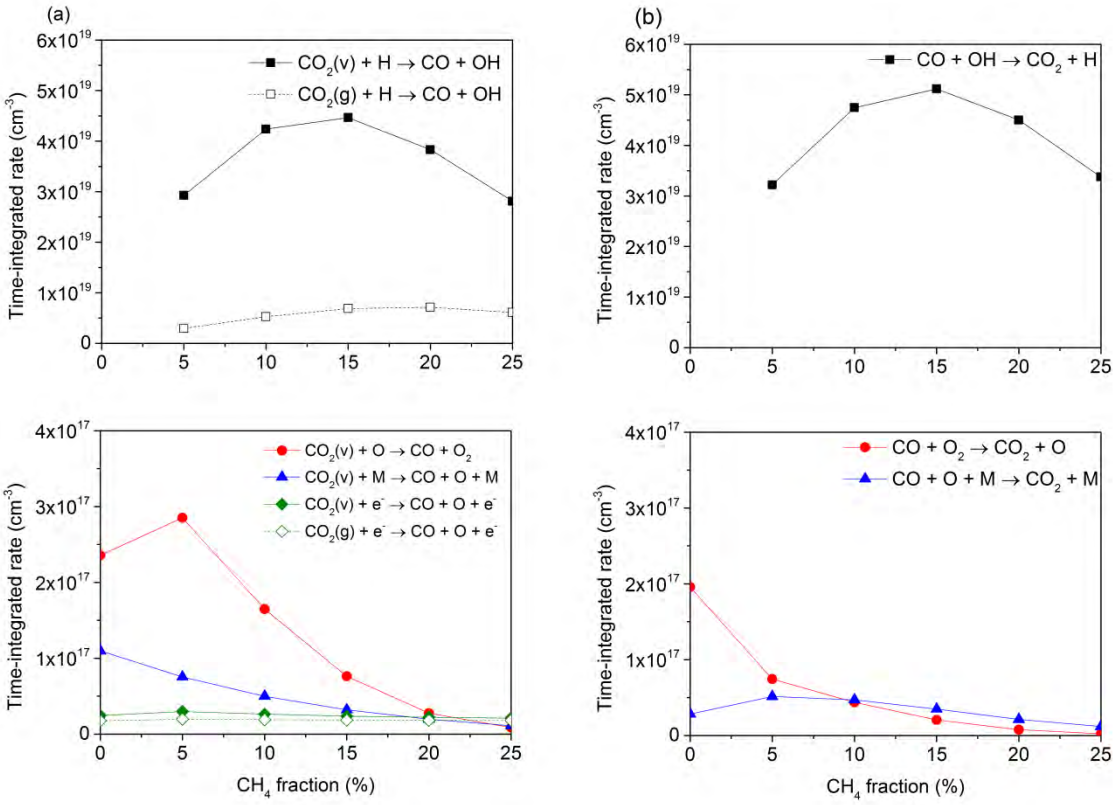

Figure S.4: Time-integrated rates of the most important loss (a) and formation (b) processes of CO_2, as a function of CH_4 fraction in the mixture.

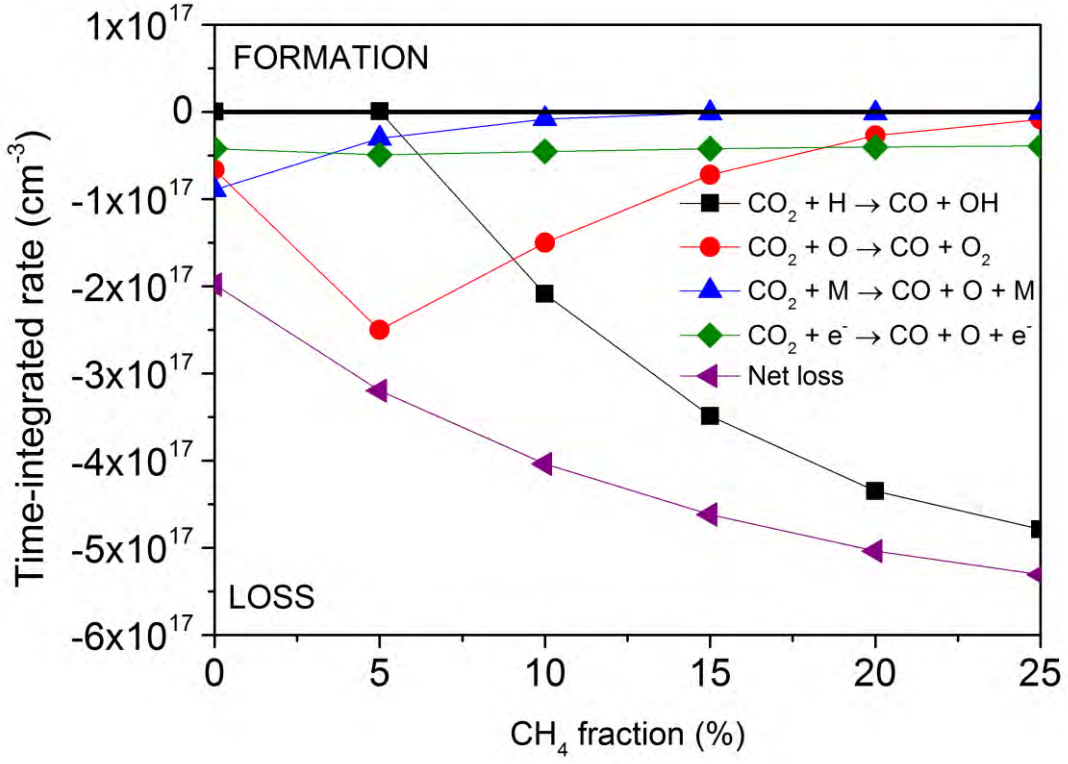

Figure S.5: Net time-integrated rates of the most important loss (and formation) processes of CO_2, as well as the total net loss rate, as a function of CH_4 fraction in the mixture. The loss processes are plotted with negative rates; the formation processes in principle with positive rates (but in this case, they are negligible).

Loss and formation of CH_4

Figure S.6 illustrates the time-integrated rates of the main loss (a) and formation (b) processes of CH_4. All the rates increase upon rising CH_4 fraction. The forward and backward reactions (i.e., loss and formation processes, respectively) are again plotted in the same color, for the sake of clarity. It is clear that for some loss rates, the backward reaction is (nearly) equally important, so we need to look again at the net rates, plotted in Figure S.7 (again in the same color). The reactions plotted as positive values contribute to the net formation of CH_4, while the reactions plotted as negative values again contribute to the net conversion (or loss) of CH_4. It is clear from Figure S.6 that some reactions yield a net formation of CH_4, especially the three-body reaction of CH_3 radicals with H atoms ($CH_3 + H + M \rightarrow CH_4 + M$), while other reactions give a net loss of CH_4, i.e., mainly the reaction of CH_4 molecules with OH or C_2H_3 radicals. The net CH_4 loss rate is also plotted. It rises with increasing CH_4 fraction, which explains why the overall (effective) CH_4 conversion indeed rises upon rising CH_4 fraction in the mixture, simply attributed to the rising CH_4 concentration.

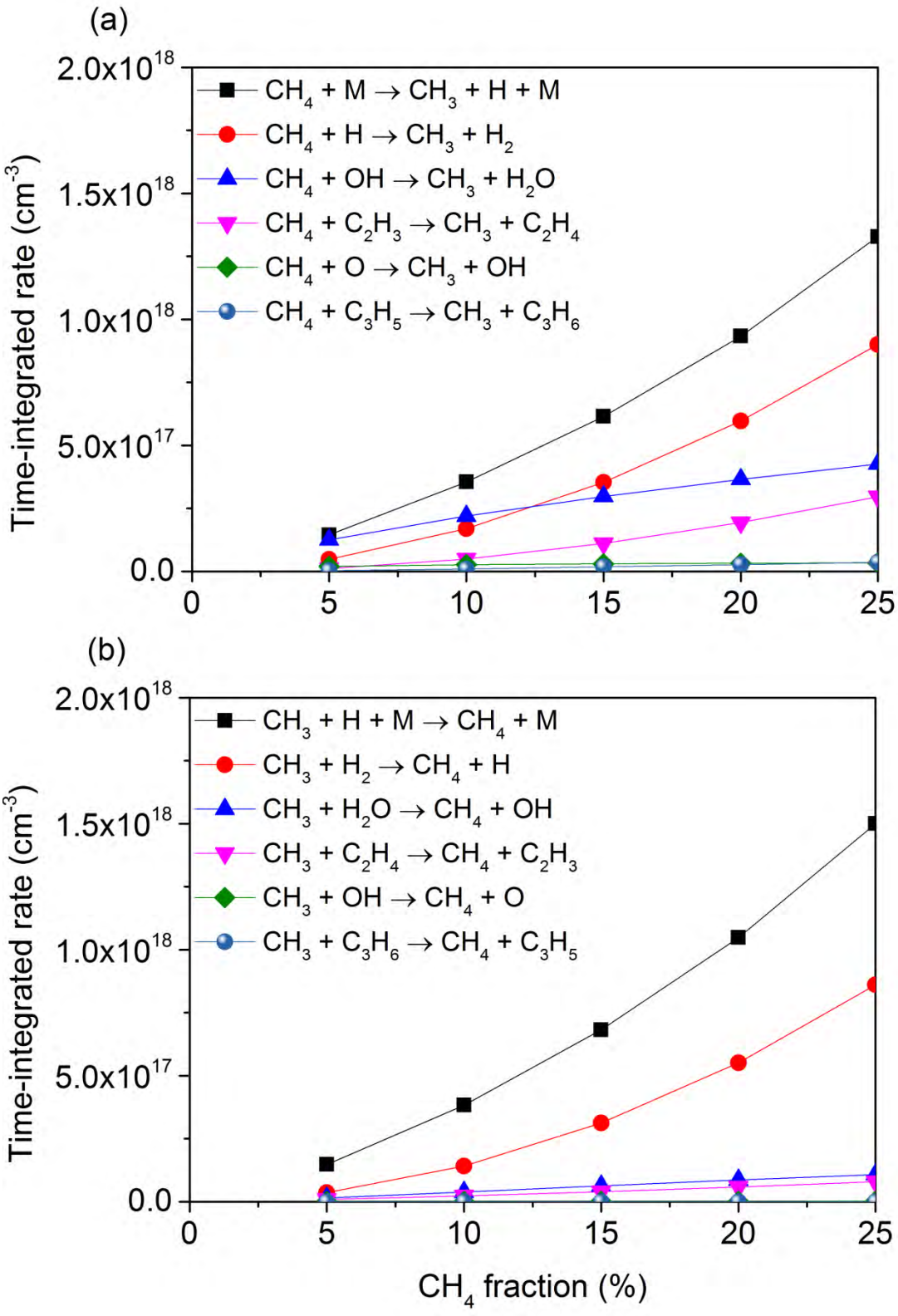

Figure S.6: Time-integrated rates of the most important loss (a) and formation (b) processes of CH_4, as a function of CH_4 fraction in the mixture.

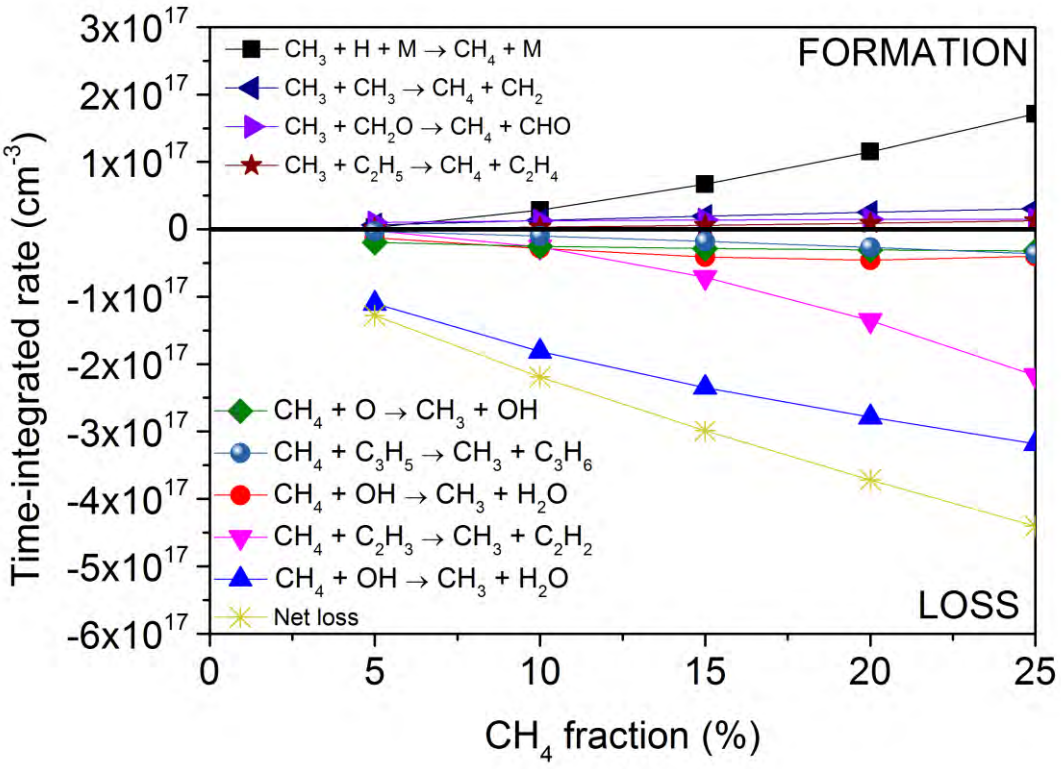

Figure S.7: Net time-integrated rates of the most important loss and formation processes of CH_4, as well as the total net loss rate, as a function of CH_4 fraction in the mixture. The loss processes are plotted with negative rates, while the formation processes are plotted with positive rates.

References

[1] N. Pinhão, A. Moura, J. B. Branco, J. Neves, *Int. J. Hydrogen Energy* **2016**, *41*, 9245–9255.

[2] S. Pancheshnyi, B. Eismann, G.J.M. Hagelaar, L.C. Pitchford, Computer code ZDPlasKin, http://www.zdplaskin.laplace.univ-tlse.fr (University of Toulouse, LAPLACE, CNRS-UPS-INP, Toulouse, France, 2008).

[3] J. M. Hagelaar, L. C. Pitchford, *Plasma Sources Sci. Technol. Plasma Sources Sci. Technol* **2005**, *14*, 722–733.

[4] A. Bogaerts, W. Wang, A. Berthelot, V. Guerra, *Plasma Sources Sci. Technol.* **2016**, *25*, 55016.

[5] M. Grofulović, L. L. Alves, V. Guerra, *J. Phys. D. Appl. Phys.* **2016**, *49*, 395207.

[6] C. De Bie, J. van Dijk, A. Bogaerts, *J. Phys. Chem. C* **2015**, *119*, 22331–22350.

[7] M. A. Lieberman, A. J. Lichtenberg, *Principles of Plasma Discharges and Materials Processing: Second Edition*, John Wiley & Sons, **2005**.

[8] G. Trenchev, S. Kolev, A. Bogaerts, *Plasma Sources Sci. Technol.* **2016**, *25*, 35014.

[9] R. Snoeckx, A. Bogaerts, *Chem. Soc. Rev.* under review.

[10] A. Fridman, *Plasma Chemistry*, Cambridge University Press, New York, **2008**.

[11] NIST Chemical Kinetics Database http://kinetics.nist.gov/kinetics/index.jsp (date: 27/02/2017).